TRAP1 (NM_016292), 5′-ACCCCAAGGATGTCGGTGA-3′ and 5′-CGGTGCGTCCGTCTTATAGTG-3′;

N-cadherin (NM_001792), 5′-CCCACAGCTCCACCATATG-AC-3′ and 5′-AAGGGAGCTCAAGGACCCAG-3′;

GAPDH (M33197), 5′-CCACTCCTCCACCTTTGACG-3′ and 5′-CACCCTGTTGCTGTAGCCAA-3′;

E2F1 (NM_005225), 5′-TGTAGGACGGTGAGAGCACTTC-3′ and 5′-TTCCCCAGGCTCACCAAAG-3′;

E2F6 (NM_198256), 5′-AGCACCAACGGACCTATCGA-3′ and 5′-TCTCAGATGAAGAGGTCCCGA-3′;

c-Myc (NM_002467), 5′-AAAGGCCCCCAAGGTAGTTATC-3′ and 5′-CGCAACAAGTCCTCTTCAGAAA-3′; and

TNFR1 (NM_001065), 5′-TTCTTGCACAGTGGACCGG-3′ and 5′-CAGAGGCTGCAATTGAAGCAC-3′.

The reaction was first incubated for 2 min at 50°C, then for 10 min at 95°C, followed by 40 cycles of 15 s at 95°C and 1 min at 60°C. Quantitative RT-PCR reactions were performed in triplicate using glyceraldehyde 3-phosphate dehydrogenase (GAPDH) as an internal control.

Luciferase reporter constructs for N-cadherin and E2F1

All PCR products were inserted into the pGL3 (R2.1)-Basic luciferase vector (Promega, Madison, WI, USA). For the N-cadherin-luciferase construct, the promoter region from −1007 to +90, relative to the transcription start site, was cloned by PCR of genomic DNA derived from SH-SY5Y cells. The E2F1-luciferase construct containing the Signal Transducers and Activator of Transcription (STAT) binding site (from −89 to +50) and the ΔSTAT-E2F1-luciferase construct (from −80 to +50) were similarly engineered. The sequences of the forward and reverse primers used are as follows:

N-cadherin, 5′-GGGGTACCTTTCCCGCAGCCCCTCCACCT-3′ and 5′-GAAGATCTAGTTTCCACCCCCTTCCCTTCCCCTCC-3′;

E2F1, 5′-GGGGTACCTTCCCGTCACGGCCGGGGCAG-3′ and 5′-GAAGATCTAGGGCTCGATCCCGCTCCGC-3′; and

ΔSTAT-E2F1, 5′-GGGGTACCCGGCCGGGGCAGCCAATTGT G-3′ and 5′-GAAGATCTAGGGCTCGATCCCGCTCCGC-3′.

Luciferase assays

For knockdown analysis, SH-SY5Y cells plated onto a 3.5 cm dish were transfected with the control phRL-TK construct (0.1 μg, Promega), N-cadherin-luciferase construct (2.5 μg) or E2F1-luciferase construct (2.5 μg) after 36 h of siRNA treatment. For the E2F1 activation assay, SH-SY5Y cells were transfected with the control phRL-TK construct (0.1 μg), N-cadherin-luciferase construct (2 μg), and HA (Hemaglutinin) construct or HA-tagged E2F1 construct (0.4 μg, a gift from Dr M. Imoto). For deletion analysis, the E2F1-luciferase construct (2.5 μg) or ΔSTAT-E2F1-luciferase construct (2.5 μg) with the control phRL-TK construct (0.1 μg) were transfected into SH-SY5Y cells. Transfection of the constructs was performed with Lipofectamine 2000 (Invitrogen) according to the manufacturer's protocol. Twenty-four hours post-transfection, luciferase activities were analyzed by a lumat LB9507 (Berthold Technologies, Bad Wildbad, Germany) using the Promega Dual-Luciferase reporter assay system. All the experiments were performed at least three times in duplicate.

Immunoprecipitation

SH-SY5Y cells were treated with 100 ng/ml TNF-α (Wako, Osaka, Japan) for 15 min at 37°C, harvested in lysis buffer (50 mM HEPES-NaOH, pH 7, 150 mM NaCl, 10% glycerol, 1.2% TritonX-100, 1.5 mM $MgCl_2$, 1 mM EGTA, 1 mM Na_3VO_4, 100 mM NaF and Protease Inhibitor Cocktail EDTA free), incubated for 20 min at 4°C and centrifuged at 17 000 *g* for 20 min at 4°C. Immunoprecipitation was carried out by incubating the supernatant with an anti-TNFR1 antibody (2 μg, Santa Cruz Biotechnology, Santa Cruz, CA, USA) or Negative Control Mouse IgG1 (2 μg, Dako, Glostrup, Denmark) with rotation at 4°C overnight followed by Protein G Sepharose 4 Fast Flow (GE Healthcare) for 2 h at 4°C. The immune complex was rinsed with wash buffer (20 mM HEPES-NaOH, pH 7, 150 mM NaCl, 10% glycerol, 0.1% TritonX-100, 1 mM Na_2VO_3) and boiled with sodium dodecyl sulfate sample buffer for 5 min.

DiI labeling

Cultured hippocampal neurons were grown to day 17 *in vitro* in a 3.5 cm poly-L-lysine–coated glass-bottomed dish (Matsunami Glass, Kishiwada, Japan), transfected with 100 nM siRNA specific to TRAP1 or control siRNA, and then incubated for 72 h. Transfected neurons were fixed with pre-warmed 4% paraformaldehyde for 30 min and washed with PBS. 1,1′-dioctadecyl-3,3,3′,3′-tetramethylindocarbocyanine perchlorate (DiI) (Invitrogen) stock solution (5 mg/ml in dimethylformamide) was diluted to 0.1 mg/ml with cod-liver oil (WAKASA, Osaka, Japan) and centrifuged for 10 min at 17 000 *g*. Each drop of the supernatant was mounted onto the soma of each neuron using FemtoJet and InjectMan NI 2 (Eppendorf, Hamburg, Germany). After 18 h of incubation, DiI labeled neurons were washed with PBS, mounted with Fluoromount (Diagnostic BioSystems, Pleasanton, CA, USA) and analyzed using a confocal laser scanning microscope (LSM-510 UV/META, Carl Zeiss, Oberkochen, Germany).

Statistical analysis

For analysis of the differences between control cells and TRAP1, TNFR1 or TNFR2 knockdown cells in the real-time RT-PCR experiment, luciferase assay, western blotting and morphological analysis of dendritic spines, statistical comparisons were performed using the unpaired Student's *t*-test. Data were considered statistically significant with values of $p < 0.05$ to control.

Genetic analysis

Subjects and methods for genetic analysis are available in the Appendix S1.

Results

TRAP1 is broadly expressed in the CNS exclusively in neurons

Because TRAP1 mRNA has been detected in whole brain lysates (Song *et al.* 1995), we examined the distribution pattern of mRNA and protein in more detail (Figs 1a and S1). *In situ* hybridization revealed that TRAP1 mRNA is broadly expressed throughout the gray matter of the brain and the spinal cord, including the regions known to be

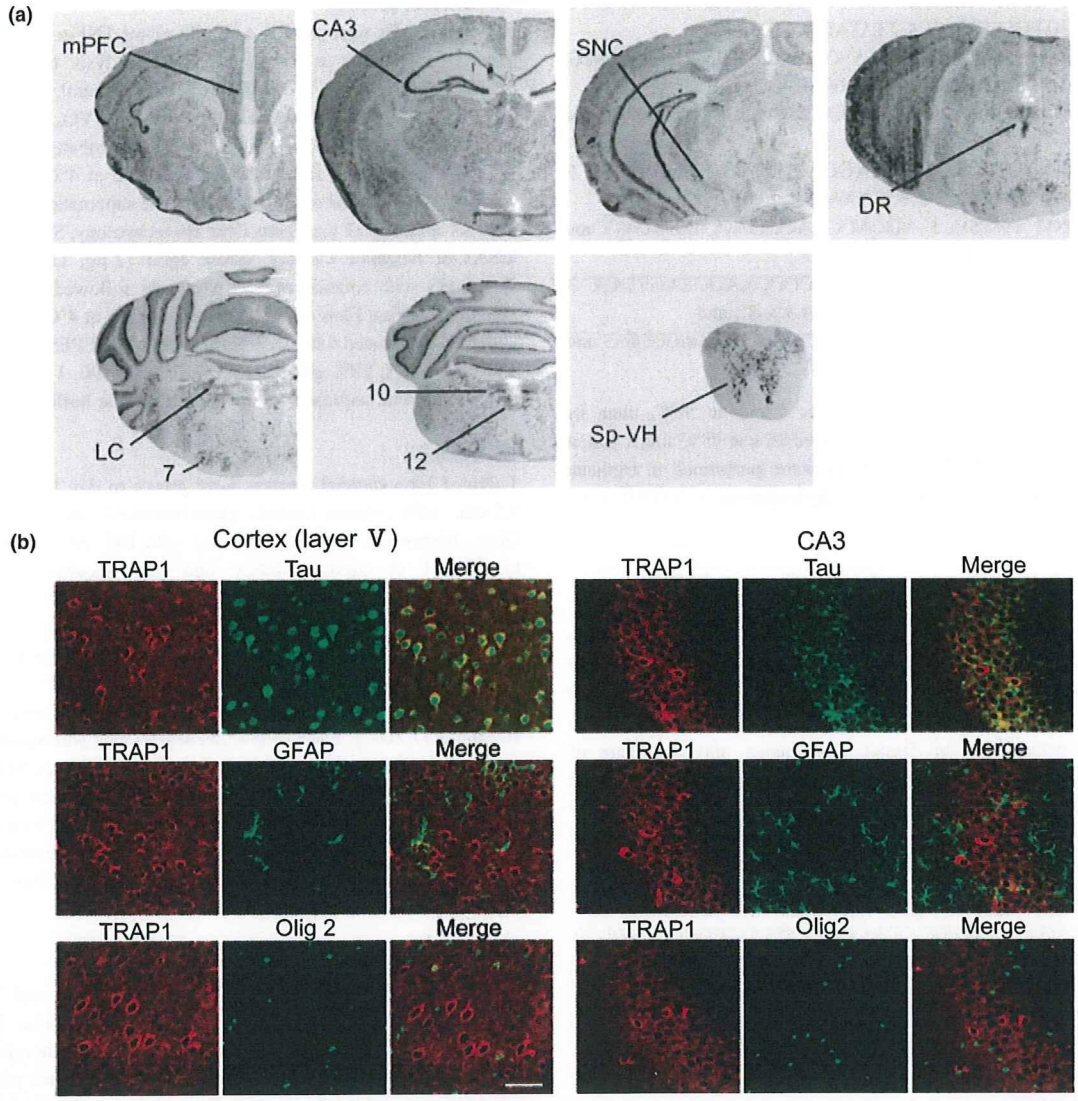

Fig. 1 Distribution of TRAP1 in the mouse brain. (a) *In situ* hybridization of TRAP1 in coronal sections of mouse brain. (b) Double immunostaining of the cortex (left panels) and CA3 of the hippocampus (right panels) with anti-TRAP1 (red), tau (green, top row), GFAP (green, middle row) and olig2 (green, bottom row) antibodies. Scale bar, 50 μm. mPFC, medial prefrontal cortex; CA3, field CA3 of the hippocampus; SNC, substantia nigra pars compacta; DR, dorsal raphe nucleus; LC, locus coeruleus; 7, facial nucleus; 10, the dorsal motor nucleus of the vagus nerve; 12, hypoglossal nucleus; Sp-VH, the ventral horn of the spinal cord; Layer V, layer V of the cortex.

affected in major depression patients, such as the medial prefrontal cortex, the hippocampus and the nuclei producing monoamine: the substantia nigra compacta, dorsal raphe nucleus and locus coeruleus (Nestler *et al.* 2002; Berton and Nestler 2006). Protein localization was also verified by immunostaining with anti-TRAP1 antibody (Fig. S1). Second, because most signals were observed within nuclei of neuron-rich brain regions, we examined whether TRAP1 is expressed predominantly in neurons. TRAP1 expressing cells were co-immunostained with a neuronal marker, tau-1, but not with an astrocyte marker, glial fibrillary acidic protein (GFAP), nor with an oligodendrocyte marker, olig2, in both cortical and hippocampal sections (Fig. 1b). Punctate immunostaining of TRAP1 was detected in the cytoplasm, which is consistent with previously reported mitochondrial localization of TRAP1 in a cell culture (Felts *et al.* 2000).

Cell adhesion is impaired in TRAP1 knockdown cells

To examine the role of TRAP1 in neuronal cells, we used the siRNAs to knockdown TRAP1 in a neuroblastoma cell line, SH-SY5Y. Western blot analysis revealed that siRNAs against TRAP1 (siTRAP1) induced a ~70% decrease of TRAP1 protein compared with that induced by a control siRNA, at 48 h after transfection (Fig. 2a). By immunocytochemistry

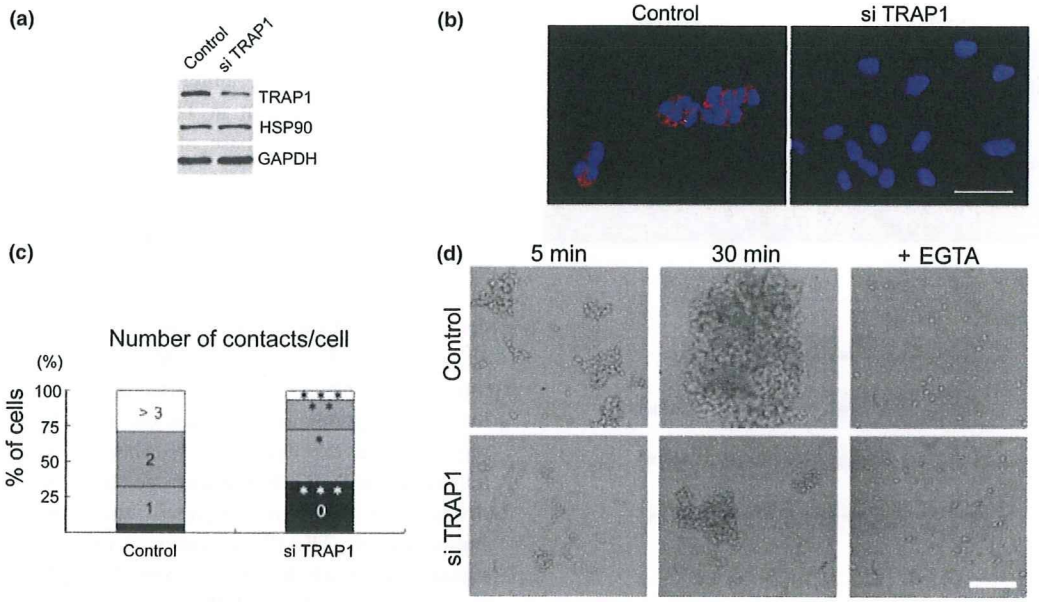

Fig. 2 TRAP1 is involved in cell-cell adhesion. (a) Immunoblotting of SH-SY5Y cells transfected with siRNAs specific to TRAP1 (siTRAP1) or control siRNAs (Control), with anti-TRAP1, HSP90 and GAPDH antibodies. Results are representative of three independent experiments. (b) Immunocytochemistry of TRAP1 knockdown and control cells with anti-TRAP1 antibody (red) and DAPI (blue). Scale bar, 50 μm. (c) Quantification of intercellular adhesion in TRAP1 knockdown cells. Asterisks indicate that the difference is statistically significant. $^{*}p < 0.05$, $^{**}p < 0.01$, $^{***}p < 0.001$ vs. control. (d) Cell-aggregation assay of TRAP1 knockdown cells. Scale bar, 200 μm.

using the same antibody, a ~80% reduction in TRAP1 protein levels by siTRAP1 was observed (Fig. 2b). The siTRAP1 targeted TRAP1 specifically, because levels of HSP90, which has sequence homologous to TRAP1 (Felts *et al.* 2000), was unaffected by the siRNAs (Fig. 2a). Upon knockdown of TRAP1, a striking cell-scattering phenotype was observed in SH-SY5Y cells; cells transfected with siTRAP1 were dispersed throughout the dish, compared to cells transfected with control siRNA that grew in aggregates resembling untransfected SH-SY5Y cells. This phenomenon was detectable as early as 24 h after transfection and became more prominent by 72 h after transfection (Fig. S2a). Immunostaining of actin filaments in the siRNA-treated cells showed no difference in cytoskeletal structure (Fig. S2b). After staining cells for actin, we quantified the percentage of cells with no inter-cellular contacts and detected a 6.2-fold increase in cells transfected with siTRAP1 (36%) compared to cells transfected with control siRNA (5.8%, Fig. 2c). Using the cell aggregation assay, TRAP1 knockdown cells showed much lower efficacy of cell-cell adhesion compared with control cells, suggesting that calcium-dependent cell adhesion is affected (Fig. 2d). These results strongly indicate that TRAP1 regulates downstream molecules crucial for cell adhesion.

N-cadherin is transcriptionally down-regulated in TRAP1 knockdown cells

We further investigated the molecular mechanism responsible for the cell scattering phenotype observed in TRAP1 knockdown cells. Expression levels of cell adhesion molecules, including N-cadherin, are directly related to the cell-scattering phenomenon (Hayashida *et al.* 2006; Yasuda *et al.* 2007) and N-cadherin mediates calcium-dependent cell adhesion in neuronal cells (Takeichi 2007). We therefore determined the expression level of N-cadherin in TRAP1 knockdown cells. We detected that N-cadherin is remarkably decreased throughout the cytoplasm, including around the membrane where cell-adhesion takes place, in the TRAP1 knockdown cells compared to control cells (Fig. 3a). Consistently, immunoblotting experiments showed that expression of N-cadherin is significantly decreased in TRAP1 knockdown cells from as early as 24 h until at least 72 h after transfection, but the expression level of β-catenin, which also regulates cell-adhesion, was unaffected (Fig. 3b). These results suggest that the cell scattering phenotype detected in TRAP1 knockdown cells is at least partially mediated by reduction of N-cadherin expression in those cells.

To determine whether cell viability or migration contributes to the cell-scattering phenotype in TRAP1 knockdown cells, we investigated cell viability by the 3-(4,5-dimethylthiazol-2-yl)-2,5-diphenyltetrazolium bromide (MTT) assay and migration by the wound healing assay (Fig. S2c and d). Although slight decrease of cell viability in TRAP1 knockdown cells was observed compared to the control cells at 48 h after transfection or later, no changes were detected at 24 h after transfection, when the cell-scattering phenotype of

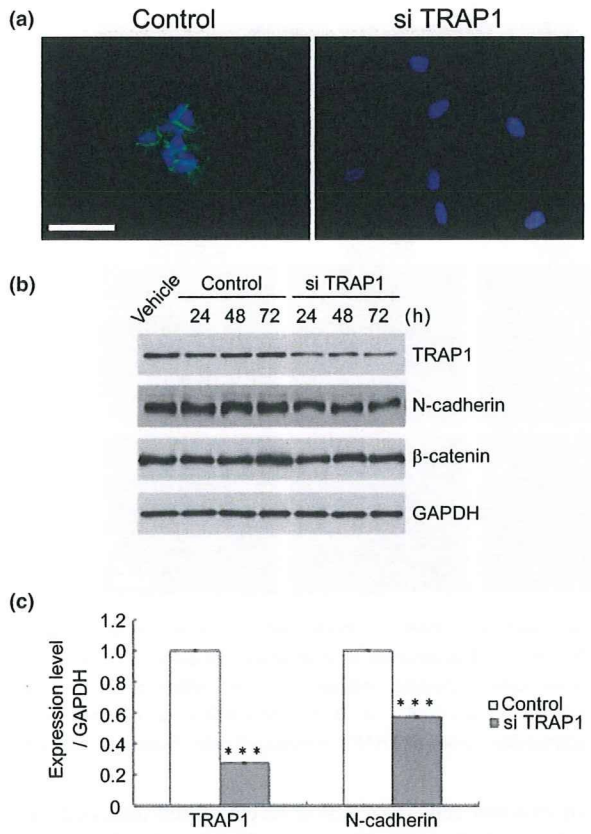

Fig. 3 TRAP1 knockdown results in the down-regulation of N-cadherin. (a) Immunocytochemistry of TRAP1 knockdown cells (right) compared with that of control cells (left) with an anti-N-cadherin antibody (green) and DAPI (blue). Scale bar, 50 μm. (b) Immunoblotting of TRAP1 knockdown cells with anti-TRAP1, N-cadherin, β-catenin and GAPDH antibodies. Results are representative of four independent experiments. (c) Quantitative RT-PCR of TRAP1 and N-cadherin mRNA levels in TRAP1 knockdown cells. GAPDH mRNA was used as an internal control. Data represent the mean ± SD ($n = 3$). ***$p < 0.001$ vs. control.

TRAP1 knockdown cells was already observed (Fig. S2a). No significant changes in the rate of cell migration were observed.

To determine if down-regulation of N-cadherin induced by siTRAP1 occurs at the transcriptional level, we measured levels of N-cadherin mRNA by real-time RT-PCR analysis 48 h after siRNA transfection and found that N-cadherin mRNA in the TRAP1 knockdown cells is about 45% lower than that in the control cells (Fig. 3c). These results indicate that TRAP1 knockdown induces transcriptional down-regulation of N-cadherin.

Taken together, these results suggest that the cell scattering phenotype in the TRAP1 knockdown cells can be mainly attributed to impaired expression of cell adhesion molecules including N-cadherin, which is transcriptionally regulated by TRAP1.

E2F1, a putative transcription factor of N-cadherin, is down-regulated in TRAP1 knockdown cells

To determine if a transcription factor is involved in down-regulation of N-cadherin in TRAP1 knockdown cells, we searched DBTSS (Database of Transcriptional Start Sites) and TRANSFAC (The Transcription Factor Database) and discovered a putative binding site for E2F1 in the promoter region of the N-cadherin gene (Fig. 4a). By immunoblot analysis and real-time PCR, we determined that the amount of both the protein and the mRNA of E2F1 were significantly decreased in TRAP1 knockdown cells (Fig. 4b and c), although the mRNA level of c-Myc, another representative transcription factor, was not affected. Next, we used the luciferase reporter assay to test our hypothesis that E2F1 regulates the expression of N-cadherin. SH-SY5Y cells transfected with the N-cadherin-luciferase plasmid showed strong activity of the reporter, and this activity was suppressed in TRAP1 knockdown cells, mimicking the signal cascade we detected *in vitro* (Fig. 4d). Furthermore, exogenously transfected E2F1 showed a 7.5-fold induction of luciferase reporter activity relative to the control vector (Fig. 4e). These results indicate that E2F1 plays a regulatory role upstream of N-cadherin in the TRAP1 knockdown cells.

Reduced phosphorylation of STAT causes down-regulation of E2F1 in TRAP1 knockdown cells

In search of an upstream molecule that regulates E2F expression, we found a recognition sequence for STAT3 located 89 bp upstream of the transcription initiation site of the E2F1 gene (Fig. 5a). Upon activation, STAT3 proteins are tyrosine-phosphorylated, dimerize and translocate to the nucleus (O'Shea *et al.* 2002). Then the nuclear phospho-STAT3 binds to STAT recognition sites located in the promoter region of downstream genes to promote the transcription of those genes. We detected that the amount of tyrosine-phosphorylated STAT3, but not the total amount of STAT3, was significantly reduced in the TRAP1 knockdown cells (Fig. 5b). Using a reporter construct containing the E2F1 promoter region fused with the luciferase gene, we found that promoter activity of the E2F1 gene was significantly reduced if the STAT3 recognition site was deleted and if TRAP1 was knocked down (Fig. 5c and d). These data indicate that TRAP1 regulates the tyrosine phosphorylation status of STAT3, which controls the expression of E2F, and thus subsequently modulates the transcription of N-cadherin.

Tyrosine phosphorylation of STAT3 and N-cadherin expression are down-regulated in TNFR1 knockdown cells

Tumor necrosis factor receptor-associated protein 1 was originally isolated as a TNFR1 binding protein using the *in vitro* binding assay (Song *et al.* 1995). We confirmed that endogenous TRAP1 was immunoprecipitated with TNFR1 in

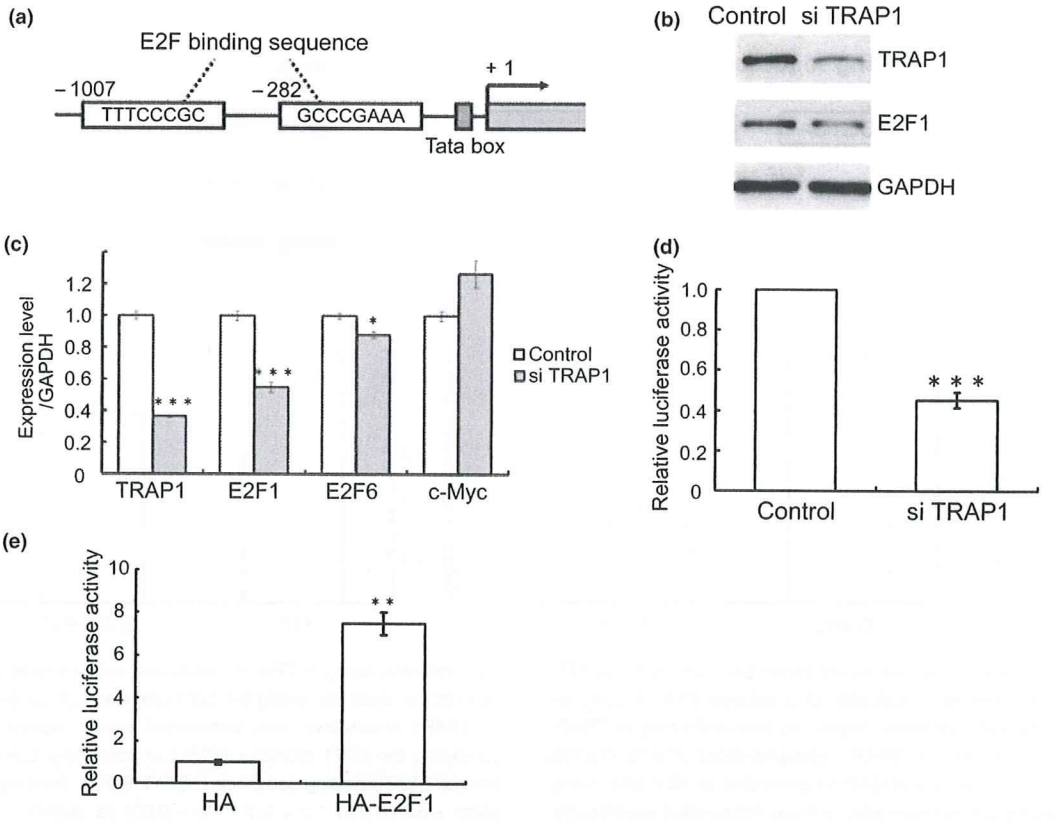

Fig. 4 TRAP1 knockdown decreases transcription activity of the N-cadherin promoter. (a) Schematic illustration of two putative E2F1 binding sequences in the regulatory region of the N-cadherin gene. (b) Immunoblotting of TRAP1 knockdown cells at 48 h after transfection with anti-TRAP1, E2F1 and GAPDH antibodies. Results are representative of three independent experiments. (c) Quantitative RT-PCR of TRAP1, E2F1, E2F6 and c-Myc mRNA levels. GAPDH mRNA was used as an internal control. Data represent the mean ± SD ($n = 3$). (d) Relative transcription activity of the N-cadherin promoter in TRAP1 knockdown cells. (e) Relative transcription activity of the N-cadherin promoter in cells transfected with HA tagged E2F1 (HA-E2F1) compared with that in cells transfected with HA (HA). Data represent the mean ± SD ($n = 3$). $^{*}p < 0.05$, $^{**}p < 0.01$, $^{***}p < 0.001$ vs. control.

SH-SY5Y cells (Fig. 6a). We next investigated whether TRAP1 is functionally associated with TNFR1.

Recently, TNF-α has been reported to activate the Jak-STAT3 pathway through TNFR1 in both peripheral cells and in the brain (Guo *et al.* 1998; Romanatto *et al.* 2007). Given that TRAP1-induced phosphorylation of STAT3 occurs downstream of TNFR1, knockdown of TNFR1 could also lead to a decrease in STAT phosphorylation. We next examined the phosphorylation status of STAT3 in the context of TNFR1 knockdown. An siRNA against TNFR1 (siTNFR1) transfected into SH-SY5Y cells effectively reduced its mRNA level (~78% compared with the control siRNA) and subsequently its protein level (Fig. 6b and c). We detected that the amount of tyrosine-phosphorylated STAT3 was significantly reduced in the TNFR1 knockdown cells (Fig. 6b). Real-time RT-PCR analysis showed decreased mRNA levels of N-cadherin in TNFR1 knockdown cells (Fig. 6c). In addition, we found that exogenous addition of TNF-α for 12 h induced N-cadherin expression (Fig. 6d). This up-regulation was completely blocked if TRAP1 or TNFR1 was knocked down using siRNA, whereas it was not altered in TNFR2 knockdowns (Fig. 6e). Taken together, these results suggest that TRAP1, which binds to the intracellular domain of TNFR1, is involved in the signal transduction pathway from TNFR1 by modulating STAT phosphorylation, resulting in the alteration of N-cadherin expression.

TRAP1 knockdown causes the down-regulation of N-cadherin and alters dendritic spine morphology in cultured hippocampal neurons

We next knocked down TRAP1 using siRNA transfection in cultured hippocampal neurons (Fig. 7a). Because N-cadherin is involved in the morphogenesis of synapses (Togashi *et al.* 2002; Okamura *et al.* 2004), we analyzed whether the morphology of dendritic spines is regulated by TRAP1 via N-cadherin in these neurons (Fig. 7b). According to a standard classification of spine morphology, spines are

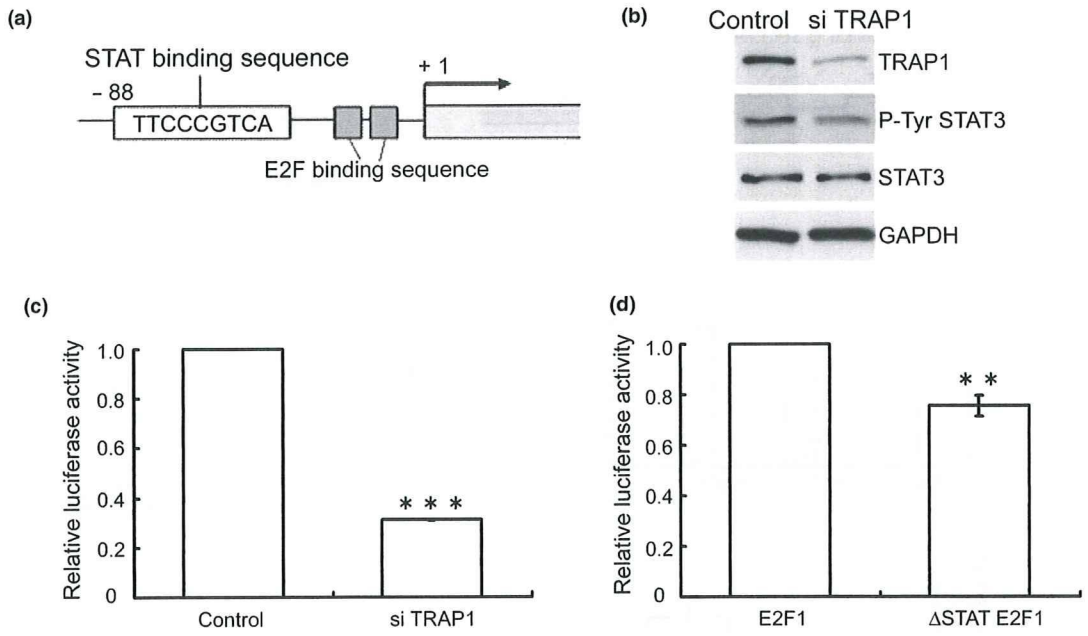

Fig. 5 TRAP1 knockdown decreases transcription activity of the E2F1 promoter. (a) Schematic illustration of a putative STAT binding sequence in the E2F1 promoter region. (b) Immunoblotting of TRAP1 knockdown cells with anti-TRAP1, phosphorylated STAT3 (Tyr705) (p-Tyr STAT3), STAT3 and GAPDH antibodies at 48 h after transfection. Results are representative of three independent experiments. (c) Luciferase assay in TRAP1 knockdown cells transfected with the reporter construct containing the E2F1 promoter. (d) Luciferase assay in TRAP1 knockdown cells transfected with a reporter construct containing the E2F1 promoter (E2F1) or containing E2F1 promoter without STAT3 binding sequence (ΔSTAT E2F1). Data represent the mean ± SD ($n = 3$). $^{**}p < 0.01$, $^{***}p < 0.001$ vs. control.

divided in two types: pedunculated and sessile; the former has a substantial stalk construction whereas the latter does not (Greg *et al.* 1999). In TRAP1 knockdown neurons, spines were predominantly sessile. Only 20.8% of spines displayed peduncular morphology compared with 66.7% in control neurons (Fig. 7c).

Association of SNPs in the *TRAP1* gene with major depression

We then examined the association between SNPs in the *TRAP1* gene and mental disorders, including schizophrenia, bipolar disorder and major depression. Six SNPs in the *TRAP1* gene selected from public databases were genotyped, and the distributions of all six SNPs were verified to be in Hardy-Weinberg proportions in all diagnostic groups (data not shown). As shown in Table 1, a statistically significant association was detected between genetic variations in the *TRAP1* gene and patients with schizophrenia (SNP3, $p = 0.048$), bipolar disorder (SNP1, $p = 0.047$), and major depression (SNP2, $p = 0.003$; SNP3, $p = 0.00086$; SNP4, $p = 0.012$; SNP5, $p = 0.0078$).

Discussion

The primary aim of this study was to elucidate the downstream pathway of TNF-α, whose role is implicated in major depression. Our SNP analyses of the *TRAP1* gene, which binds to the receptor of TNF-α, suggested that the *TRAP1* gene *per se* or another gene in linkage disequilibrium might be associated with psychiatric disorders, particularly with major depression. We showed that TRAP1 is expressed in brain neurons including those in regions closely related to the symptoms of depression (Nestler *et al.* 2002; Berton and Nestler 2006). We further demonstrated that TRAP1 regulates the expression of N-cadherin in the TNF-α/TNFR1 signaling pathway, via regulation of STAT3 tyrosine phosphorylation and E2F expression, resulting in alterations of cell-adhesion efficacy, which causes a morphological change of dendritic spines in cultured hippocampal neurons.

In the CNS, TNF-α is known to be produced by neurons, as well as by astrocytes and microglia (Pan *et al.* 1997). The expression of TNFR1 and TNFR2 in the CNS has also been reported (Bette *et al.* 2003). Although TNFR2 is expressed in non-neuronal cells, TNFR1 is constitutively and broadly expressed in many neurons in the CNS. High levels of TNFR1 expression has been documented in the forebrain regions and in several motor nuclei in the brainstem (Bette *et al.* 2003). Our immunohistochemical analyses showed that the expression pattern of TRAP1 is strikingly similar to that of TNFR1, suggesting that TRAP1 works synergistically with TNFR1 in the brain and contributes to neuronal

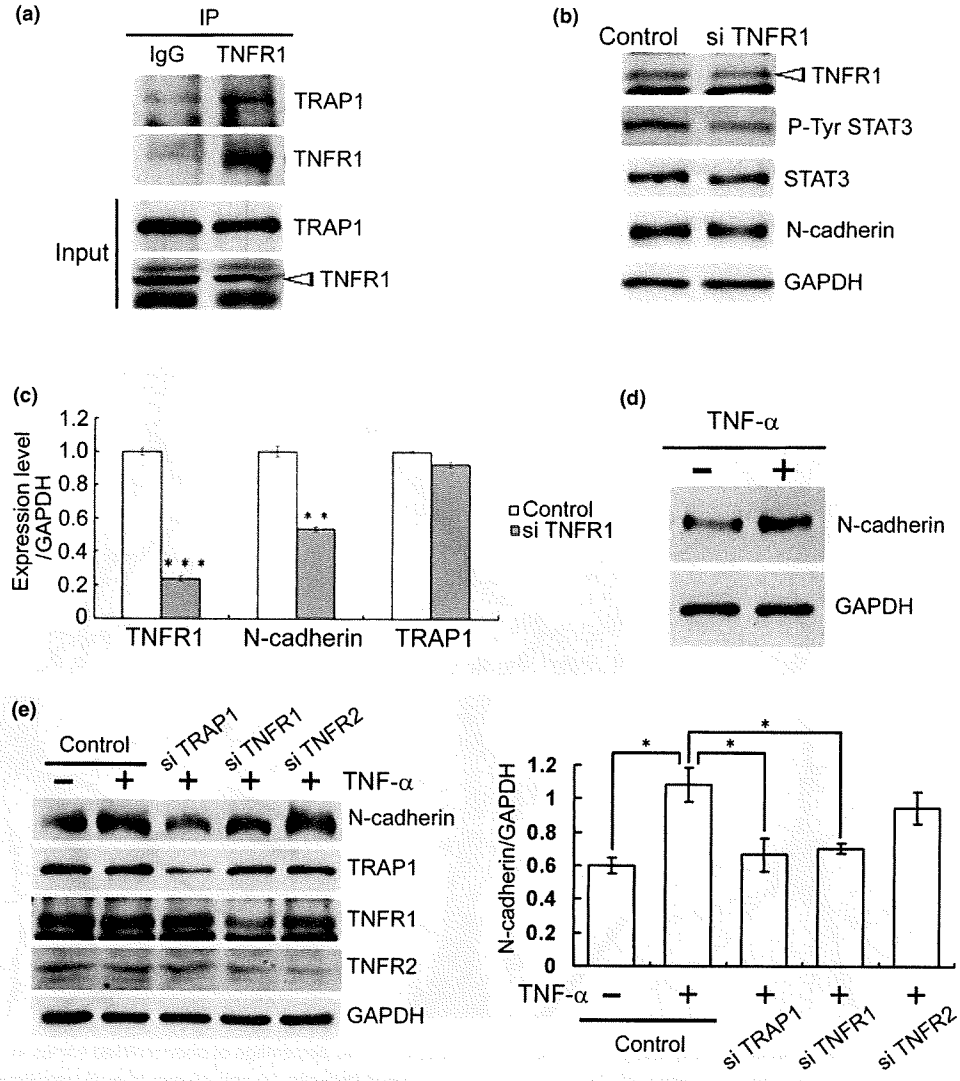

Fig. 6 TRAP1 binds TNFR1 and is involved in N-cadherin expression and phosphorylation of STAT3. (a) Immunoprecipitation of endogenous TNFR1 with endogenous TRAP1 after 15 min of incubation with TNF-α in SH-SY5Y cells. (b) TNFR1 knockdown results in a reduced expression of N-cadherin and tyrosine-phosphorylated STAT3 at 48 h after transfection. (c) Quantitative RT-PCR of TNFR1, N-cadherin and TRAP1 mRNA levels in TNFR1 knockdown. GAPDH mRNA was used as an internal control. (d) TNF-α (100 ng/ml) increases N-cadherin expression at 12 h after treatment. Results are representative of four independent experiments. (e) Knocking down TRAP1 or TNFR1 inhibits N-cadherin up-regulation by TNF-α. GAPDH was used as an internal control. Data represent the mean ± SD ($n = 3$). $^{*}p < 0.05$, $^{**}p < 0.01$, $^{***}p < 0.001$ vs. control.

function. N-cadherin is also expressed in neurons in the adult mouse brain (Redies and Takeichi 1993; Barami *et al.* 1994; Takeichi 2007). Thus, our data verified the co-expression of TNFR1, TRAP1 and N-cadherin in neurons in the brain.

Type I tumor necrosis factor receptor (TNFR1) is localized in the plasma membrane to transmit extracellular TNF-α signals to the intracellular compartment. We have shown that TRAP1 is distributed throughout the cytoplasm including areas near the membrane, and that TRAP1 immunoprecipitates with TNFR1. In addition, we showed that knocking down TNFR1 or TRAP1 has similar effects on N-cadherin expression. Moreover, up-regulation of N-cadherin induced by TNF-α was blocked in TRAP1 or TNFR1 knockdowns. Together, these data indicate that TRAP1 interacts with TNFR1 to modulate cell adhesion.

Considering that mitochondrial TRAP1 undergoes phosphorylation by PINK1 and inhibits cytochrome *c* release from mitochondria (Abeliovich 2007; Pridgeon *et al.* 2007; Mills *et al.* 2008), it is likely that TRAP1 interacts with proteins in various cellular compartments to exert multifaceted functions in the brain, like other members of the HSP90 family (Csermely *et al.* 1998; Pratt 1998).

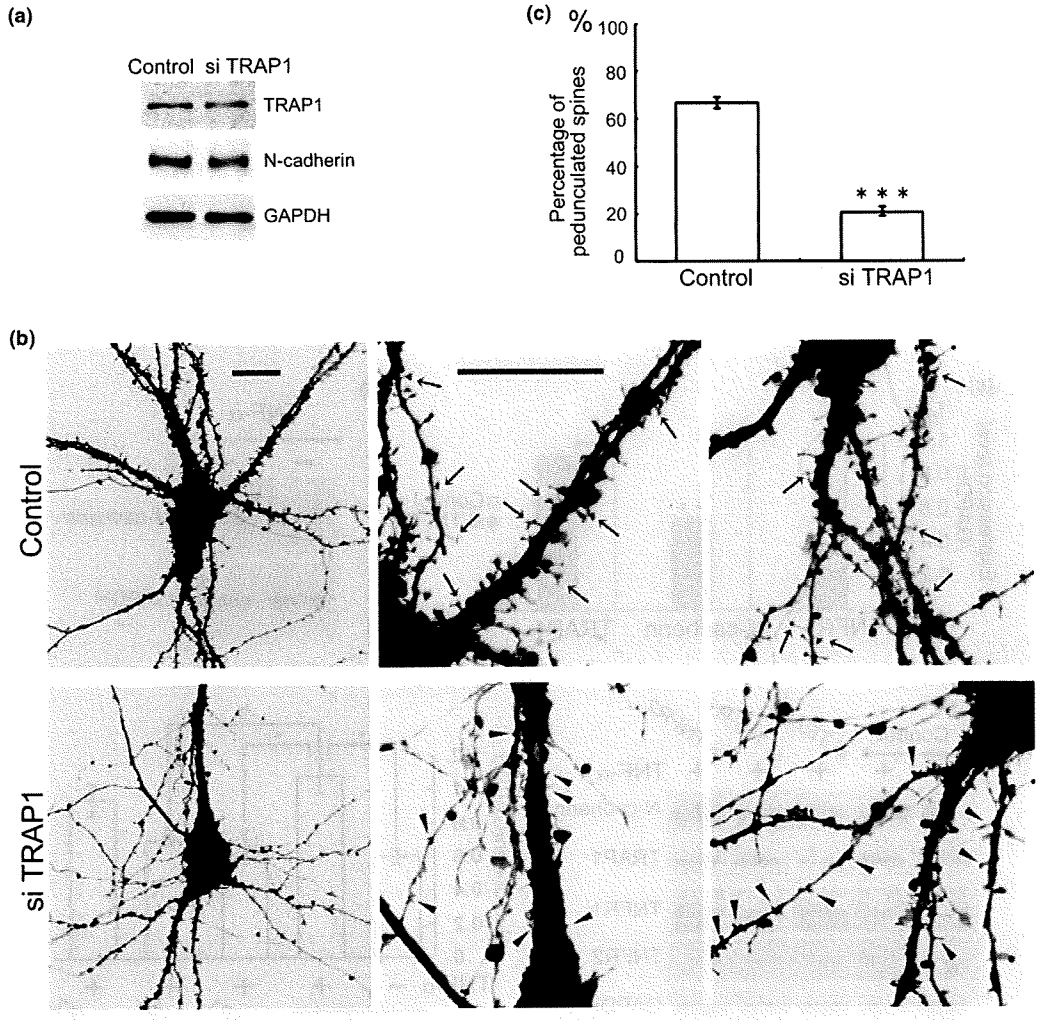

Fig. 7 TRAP1 knockdown alters dendritic morphology in cultured primary hippocampal neurons. (a) Immunoblotting of TRAP1, N-cadherin and GAPDH in TRAP1 knockdown neurons. (b) DiI images of TRAP1 knockdown neurons and control neurons at DIV21. Scale bar, 20 μm. (c) The percentage of pedunculated spines in total spines that are located between 10 and 40 mm from the proximal origin of dendrites in seven each neurons. Data represent the mean ± SD. ***$p < 0.001$ vs. control.

Gene manipulation studies in mice have revealed that a defect in either TNF-α, TNFR1 or cell adhesion molecules has a significantly effects emotional behavior (Manabe *et al.* 2000; Yamada *et al.* 2000; Simen *et al.* 2006). In particular, TNFR1 knockout mice show anti-depression-like behavior (Simen *et al.* 2006). However, little is known about the relationship between TNF-α and cell adhesion molecules in the CNS, although *in vitro* studies in epithelial cells have suggested the involvement of TNF-α in the regulation of cell adhesion molecules (Pober *et al.* 1986; Lassalle *et al.* 1993; Dobbie *et al.* 1999; Young *et al.* 2002). Interestingly, TNF-α-induced over-expression of adhesion molecules has been implicated in the pathogenesis of rheumatoid arthritis, which is frequently accompanied by major depression (Bacon *et al.* 2002; Hurlimann *et al.* 2002; Gonzalez-Juanatey *et al.* 2004). In the present study, we showed that TNF-α up-regulates N-cadherin expression in neuronal cells, thus providing a possible link between TNF-α over-expression and impaired brain functions.

Recent studies have indicated that N-cadherin is an important regulator of synaptic morphology and function (Okamura *et al.* 2004; Tanabe *et al.* 2006; Takeichi 2007). Disrupting N-cadherin in hippocampal neurons with a dominant negative mutant results in altered dendritic spine morphology and aberrant synaptic organization (Togashi *et al.* 2002). Functionally, N-cadherin regulates synaptic plasticity; activity dependent accumulation of N-cadherin at the synapse is essential for spine remodeling and long-term potentiation (Tang *et al.* 1998; Bozdagi *et al.* 2000; Tanaka *et al.* 2000). In addition, activity dependent

Table 1 Allele distributions for six SNPs in the TRAP1 gene among patients with schizophrenia, bipolar disorder and major depression and controls

SNP-ID	dbSNP	Distance from SNP1	Major/ Minor	Location	Cont, $n = 785$	Schizophrenia, $n = 698$			Bipolar disorder, $n = 91$			Major depression, $n = 361$		
							p	OR		p	OR		p	OR
SNP1	rs6500552		T/C	intron1	0.322	0.309	0.45	–	0.396	0.047	1.38	0.328	0.78	–
SNP2	rs1639150	12 189	T/C	intron1	0.45	0.441	0.62	–	0.445	0.91	–	0.384	0.003	0.76
SNP3	rs2108430	21 315	T/C	intron3	0.493	0.529	0.048	1.16	0.527	0.38	–	0.568	0.00086	1.35
SNP4	rs13926	34 928	C/G	exon9 (R307G)	0.496	0.423	0.88	–	0.401	0.52	–	0.482	0.012	1.25
SNP5	rs1136948	37 620	C/G	exon11 (D395E)	0.126	0.107	0.1	–	0.143	0.54	–	0.089	0.0078	0.67
SNP6	rs710891	49 296	T/C	intron16	0.454	0.467	0.48	–	0.429	0.51	–	0.485	0.172	–

Minor allele frequencies in controls are shown. Cont, control; OR, odds ratio.

α-amino-3-hydroxy-5-methylisoxazole-4-propionate (AMPA) receptor trafficking to the synaptic membrane, which is thought to be the molecular basis of learning and memory, is also regulated by N-cadherin (Nuriya and Huganir 2006). These facts indicate that N-cadherin plays important roles in higher brain functions and altered expression of N-cadherin presumably is associated with the pathogenesis of mental disorders. Indeed, N-cadherin is up-regulated in hippocampal neurons by contextual fear conditioning and its dimerization is critical for normal contextual memory formation via the extracellular signal-regulated kinase (ERK) signaling cascade (Schrick *et al.* 2007), also implicated in the pathogenesis of major depression (Dwivedi *et al.* 2001; Coyle and Duman 2003; Einat *et al.* 2003; Hashimoto *et al.* 2006). Our results provide another line of evidence that the signal transduction pathway modulating N-cadherin expression induces morphological changes at synapses, which in turn, plays a key role in cognitive function.

We showed that four SNPs in the *TRAP1* gene may be associated with the pathogenesis of mental disorders, particularly major depression, including two SNPs that cause an amino acid change in the TRAP1 protein: R307G (rs13926) and D395E (rs1136948). Our preliminary study showed that these two non-synonymous SNPs are located in the region critical for the binding of TRAP1 to TNFR1, suggesting that the binding affinity of TRAP1 to TNFR1 or the downstream signaling of TRAP1 might be altered (data not shown). Intronic SNPs have been known to affect alternative splicing, and therefore can be pathogenic (Medina *et al.* 2008; Weickert *et al.* 2008). Functional analysis of SNPs in the *TRAP1* gene, in addition to considering the possibility of linkage disequilibrium is required to clarify the involvement of TRAP1 in the pathogenesis of major depression.

In conclusion, this study provides new and important information towards understanding the causal connections between TNF-α and synaptic function via cell adhesion molecules such as N-cadherin. These findings have important implications for revealing the molecular basis of the pathogenesis of psychiatric disorders, especially major depression, and for future therapeutic interventions for these disorders.

Acknowledgements

The authors thank Dr Masaya Imoto for supplying HA-tagged E2F1, Drs Hidekazu Tanaka, Ko Okamura and Keisuke Sako for technical advice, Drs H Akiko Popiel, Mika Nakamoto and Lisa A. McGraw for critical reading of the manuscript and Akemi Arakawa, Dr Manabu Taniguchi and Yoshihisa Koyama for technical assistance. This study was partly supported by a Grant-in-Aid for Scientific Research from the Ministry of Education, Culture, Sports, Science and Technology of Japan, and a Research Fellowship from the Japan Society for the Promotion of Science for Young Scientists (K.K.).

Supporting Information

Additional Supporting Information may be found in the online version of this article:

Appendix S1 Materials and methods.

Figure S1 Immunohistochemical analysis of TRAP1 in the mouse brain.

Figure S2 (a) Temporal profile of scattered phenotype in TRAP1 knockdown SH-SY5Y cells. Scale bar, 125 μm. (b) Fluorescence images of F-actin in TRAP1 knockdown cells and control cells. Scale bar, 50 μm. (c) Proliferation assay of TRAP1 knockdown cells. (d) Cell migration assay of TRAP1 knockdown cells. Scale bar, 500 μm.

Please note: Wiley-Blackwell are not responsible for the content or functionality of any supporting materials supplied by the authors. Any queries (other than missing material) should be directed to the corresponding author for the article.

References

Abeliovich A. (2007) Parkinson's disease: pro-survival effects of PINK1. *Nature* **448**, 759–760.

Bacon P. A., Stevens R. J., Carruthers D. M., Young S. P. and Kitas G. D. (2002) Accelerated atherogenesis in autoimmune rheumatic diseases. *Autoimmun. Rev.* **1**, 338–347.

Barami K., Kirschenbaum B., Lemmon V. and Goldman S. A. (1994) N-cadherin and Ng-CAM/8D9 are involved serially in the migration of newly generated neurons into the adult songbird brain. *Neuron* **13**, 567–582.

Baud V. and Karin M. (2001) Signal transduction by tumor necrosis factor and its relatives. *Trends Cell Biol.* **11**, 372–377.

Berton O. and Nestler E. J. (2006) New approaches to antidepressant drug discovery: beyond monoamines. *Nat. Rev. Neurosci.* **7**, 137–151.

Bette M., Kaut O., Schafer M. K. and Weihe E. (2003) Constitutive expression of p55TNFR mRNA and mitogen-specific up-regulation of TNF alpha and p75TNFR mRNA in mouse brain. *J. Comp. Neurol.* **465**, 417–430.

Bozdagi O., Shan W., Tanaka H., Benson D. L. and Huntley G. W. (2000) Increasing numbers of synaptic puncta during late-phase LTP: N-cadherin is synthesized, recruited to synaptic sites, and required for potentiation. *Neuron* **28**, 245–259.

Chen C. F., Chen Y., Dai K., Chen P. L., Riley D. J. and Lee W. H. (1996) A new member of the hsp90 family of molecular chaperones interacts with the retinoblastoma protein during mitosis and after heat shock. *Mol. Cell. Biol.* **16**, 4691–4699.

Coyle J. T. and Duman R. S. (2003) Finding the intracellular signaling pathways affected by mood disorder treatments. *Neuron* **38**, 157–160.

Csermely P., Schnaider T., Soti C., Prohaszka Z. and Nardai G. (1998) The 90-kDa molecular chaperone family: structure, function, and clinical applications. A comprehensive review. *Pharmacol. Ther.* **79**, 129–168.

Dobbie M. S., Hurst R. D., Klein N. J. and Surtees R. A. (1999) Upregulation of intercellular adhesion molecule-1 expression on human endothelial cells by tumour necrosis factor-alpha in an in vitro model of the blood-brain barrier. *Brain Res.* **830**, 330–336.

Dwivedi Y., Rizavi H. S., Roberts R. C., Conley R. C., Tamminga C. A. and Pandey G. N. (2001) Reduced activation and expression of ERK1/2 MAP kinase in the post-mortem brain of depressed suicide subjects. *J. Neurochem.* **77**, 916–928.

Einat H., Yuan P., Gould T. D., Li J., Du J., Zhang L., Manji H. K. and Chen G. (2003) The role of the extracellular signal-regulated kinase signaling pathway in mood modulation. *J. Neurosci.* **23**, 7311–7316.

Felts S. J., Owen B. A., Nguyen P., Trepel J., Donner D. B. and Toft D. O. (2000) The hsp90-related protein TRAP1 is a mitochondrial protein with distinct functional properties. *J. Biol. Chem.* **275**, 3305–3312.

Furukawa T., Kozak C. A. and Cepko C. L. (1997) *rax*, a novel paired-type homeobox gene, shows expression in the anterior neural fold and developing retina. *Proc. Natl Acad. Sci. USA* **94**, 3088–3093.

Gonzalez-Juanatey C., Testa A., Garcia-Castelo A., Garcia-Porrua C., Llorca J. and Gonzalez-Gay M. A. (2004) Active but transient improvement of endothelial function in rheumatoid arthritis patients undergoing long-term treatment with anti-tumor necrosis factor alpha antibody. *Arthritis Rheum.* **51**, 447–450.

Greg S., Nelson S. and Michael H. (1999) *Dendrites*. Oxford University Press, New York

Guo D., Dunbar J. D., Yang C. H., Pfeffer L. M. and Donner D. B. (1998) Induction of Jak/STAT signaling by activation of the type 1 TNF receptor. *J. Immunol.* **160**, 2742–2750.

Hashimoto R., Numakawa T., Ohnishi T. *et al.* (2006) Impact of the DISC1 Ser704Cys polymorphism on risk for major depression, brain morphology and ERK signaling. *Hum. Mol. Genet.* **15**, 3024–3033.

Hayashida Y., Urata Y., Muroi E., Kono T., Miyata Y., Nomata K., Kanetake H., Kondo T. and Ihara Y. (2006) Calreticulin represses E-cadherin gene expression in Madin-Darby canine kidney cells via Slug. *J. Biol. Chem.* **281**, 32469–32484.

Hestad K. A., Tonseth S., Stoen C. D., Ueland T. and Aukrust P. (2003) Raised plasma levels of tumor necrosis factor alpha in patients with depression: normalization during electroconvulsive therapy. *J. Ect.* **19**, 183–188.

Hurlimann D., Forster A., Noll G. *et al.* (2002) Anti-tumor necrosis factor-alpha treatment improves endothelial function in patients with rheumatoid arthritis. *Circulation* **106**, 2184–2187.

Irwin M. R. and Miller A. H. (2007) Depressive disorders and immunity: 20 years of progress and discovery. *Brain Behav. Immun.* **21**, 374–383.

Jun T. Y., Pae C. U., Hoon H., Chae J. H., Bahk W. M., Kim K. S. and Serretti A. (2003) Possible association between -G308A tumour necrosis factor-alpha gene polymorphism and major depressive disorder in the Korean population. *Psychiatr. Genet.* **13**, 179–181.

Karin M. and Lin A. (2002) NF-kappaB at the crossroads of life and death. *Nat. Immunol.* **3**, 221–227.

Kubota K., Kumamoto N., Matsuzaki S. *et al.* (2009) Dysbindin engages in c-Jun N-terminal kinase activity and cytoskeletalorganization. *Biochem. Biophys. Res. Commun.* **379**, 191–195.

Lanquillon S., Krieg J. C., Bening-Abu-Shach U. and Vedder H. (2000) Cytokine production and treatment response in major depressive disorder. *Neuropsychopharmacology* **22**, 370–379.

Lassalle P., Gosset P., Delneste Y., Tsicopoulos A., Capron A., Joseph M. and Tonnel A. B. (1993) Modulation of adhesion molecule expression on endothelial cells during the late asthmatic reaction: role of macrophage-derived tumour necrosis factor-alpha. *Clin. Exp. Immunol.* **94**, 105–110.

Manabe T., Togashi H., Uchida N. *et al.* (2000) Loss of cadherin-11 adhesion receptor enhances plastic changes in hippocampal synapses and modifies behavioral responses. *Mol. Cell. Neurosci.* **15**, 534–546.

Medina M. W., Gao F., Ruan W., Rotter J. I. and Krauss R. M. (2008) Alternative splicing of 3-hydroxy-3-methylglutaryl coenzyme A reductase is associated with plasma low-density lipoprotein cholesterol response to simvastatin. *Circulation* **118**, 355–362.

Mills R. D., Sim C. H., Mok S. S., Mulhern T. D., Culvenor J. G. and Cheng H. C. (2008) Biochemical aspects of the neuroprotective mechanism of Pten-induced kinase-1 (Pink1). *J. Neurochem.* **105**, 18–33.

Nestler E. J., Barrot M., DiLeone R. J., Eisch A. J., Gold S. J. and Monteggia L. M. (2002) Neurobiology of depression. *Neuron* **34**, 13–25.

Nuriya M. and Huganir R. L. (2006) Regulation of AMPA receptor trafficking by N-cadherin. *J. Neurochem.* **97**, 652–661.

O'Shea J. J., Gadina M. and Schreiber R. D. (2002) Cytokine signaling in 2002: new surprises in the Jak/Stat pathway. *Cell* **109**(Suppl), S121–S131.

Okamura K., Tanaka H., Yagita Y., Saeki Y., Taguchi A., Hiraoka Y., Zeng L. H., Colman D. R. and Miki N. (2004) Cadherin activity is required for activity-induced spine remodeling. *J. Cell Biol.* **167**, 961–972.

Pan W., Zadina J. E., Harlan R. E., Weber J. T., Banks W. A. and Kastin A. J. (1997) Tumor necrosis factor-alpha: a neuromodulator in the CNS. *Neurosci. Biobehav. Rev.* **21**, 603–613.

Pober J. S., Gimbrone Jr M. A., Lapierre L. A., Mendrick D. L., Fiers W., Rothlein R. and Springer T. A. (1986) Overlapping patterns of activation of human endothelial cells by interleukin 1, tumor necrosis factor, and immune interferon. *J. Immunol.* **137**, 1893–1896.

Pratt W. B. (1998) The hsp90-based chaperone system: involvement in signal transduction from a variety of hormone and growth factor receptors. *Proc. Soc. Exp. Biol. Med.* **217**, 420–434.

Pridgeon J. W., Olzmann J. A., Chin L. S. and Li L. (2007) PINK1 protects against oxidative stress by phosphorylating mitochondrial chaperone TRAP1. *PLoS Biol.* **5**, e172.

Redies C. and Takeichi M. (1993) Expression of N-cadherin mRNA during development of the mouse brain. *Dev. Dyn.* **197**, 26–39.

Reichenberg A., Yirmiya R., Schuld A., Kraus T., Haack M., Morag A. and Pollmacher T. (2001) Cytokine-associated emotional and cognitive disturbances in humans. *Arch. Gen. Psychiatry* **58**, 445–452.

Romanatto T., Cesquini M., Amaral M. E., Roman E. A., Moraes J. C., Torsoni M. A., Cruz-Neto A. P. and Velloso L. A. (2007) TNF-alpha acts in the hypothalamus inhibiting food intake and increasing the respiratory quotient–effects on leptin and insulin signaling pathways. *Peptides* **28**, 1050–1058.

Schrick C., Fischer A., Srivastava D. P., Tronson N. C., Penzes P. and Radulovic J. (2007) N-cadherin regulates cytoskeletally associated IQGAP1/ERK signaling and memory formation. *Neuron* **55**, 786–798.

Simen B. B., Duman C. H., Simen A. A. and Duman R. S. (2006) TNFalpha signaling in depression and anxiety: behavioral consequences of individual receptor targeting. *Biol. Psychiatry* **59**, 775–785.

Simmons A. D., Musy M. M., Lopes C. S., Hwang L. Y., Yang Y. P. and Lovett M. (1999) A direct interaction between EXT proteins and glycosyltransferases is defective in hereditary multiple exostoses. *Hum. Mol. Genet.* **8**, 2155–2164.

Song H. Y., Dunbar J. D., Zhang Y. X., Guo D. and Donner D. B. (1995) Identification of a protein with homology to hsp90 that binds the type 1 tumor necrosis factor receptor. *J. Biol. Chem.* **270**, 3574–3581.

Takeichi M. (2007) The cadherin superfamily in neuronal connections and interactions. *Nat. Rev. Neurosci.* **8**, 11–20.

Takeichi M. and Nakagawa S. (2001) Cadherin-dependent cell-cell adhesion. *Curr. Protoc. Cell Biol.* Chapter 9, Unit 9.3.

Tanabe K., Takahashi Y., Sato Y., Kawakami K., Takeichi M. and Nakagawa S. (2006) Cadherin is required for dendritic morphogenesis and synaptic terminal organization of retinal horizontal cells. *Development* **133**, 4085–4096.

Tanaka H., Shan W., Phillips G. R., Arndt K., Bozdagi O., Shapiro L., Huntley G. W., Benson D. L. and Colman D. R. (2000) Molecular modification of N-cadherin in response to synaptic activity. *Neuron* **25**, 93–107.

Tang L., Hung C. P. and Schuman E. M. (1998) A role for the cadherin family of cell adhesion molecules in hippocampal long-term potentiation. *Neuron* **20**, 1165–1175.

Togashi H., Abe K., Mizoguchi A., Takaoka K., Chisaka O. and Takeichi M. (2002) Cadherin regulates dendritic spine morphogenesis. *Neuron* **35**, 77–89.

Tuglu C., Kara S. H., Caliyurt O., Vardar E. and Abay E. (2003) Increased serum tumor necrosis factor-alpha levels and treatment response in major depressive disorder. *Psychopharmacology (Berl)* **170**, 429–433.

Wallach D., Varfolomeev E. E., Malinin N. L., Goltsev Y. V., Kovalenko A. V. and Boldin M. P. (1999) Tumor necrosis factor receptor and Fas signaling mechanisms. *Annu. Rev. Immunol.* **17**, 331–367.

Weickert C. S., Miranda-Angulo A. L., Wong J., Perlman W. R., Ward S. E., Radhakrishna V., Straub R. E., Weinberger D. R. and Kleinman J. E. (2008) Variants in the estrogen receptor alpha gene and its mRNA contribute to risk for schizophrenia. *Hum. Mol. Genet.* **17**, 2293–2309.

Yamada K., Iida R., Miyamoto Y., Saito K., Sekikawa K., Seishima M. and Nabeshima T. (2000) Neurobehavioral alterations in mice with a targeted deletion of the tumor necrosis factor-alpha gene: implications for emotional behavior. *J. Neuroimmunol.* **111**, 131–138.

Yasuda S., Tanaka H., Sugiura H. *et al.* (2007) Activity-induced protocadherin arcadlin regulates dendritic spine number by triggering N-cadherin endocytosis via TAO2beta and p38 MAP kinases. *Neuron* **56**, 456–471.

Young J. L., Libby P. and Schonbeck U. (2002) Cytokines in the pathogenesis of atherosclerosis. *Thromb. Haemost.* **88**, 554–567.

Neuroscience 163 (2009) 1146–1157

THE DISTRIBUTION AND CHARACTERIZATION OF ENDOGENOUS PROTEIN ARGININE N-METHYLTRANSFERASE 8 IN MOUSE CNS

A. KOUSAKA,[a] Y. MORI,[a]* Y. KOYAMA,[a] T. TANEDA,[a] S. MIYATA[a,b] AND M. TOHYAMA[a,b]

[a]*Department of Anatomy and Neuroscience, Graduate School of Medicine, The Osaka-Hamamatsu Joint Research Center for Child Mental Development, Osaka University, 2-2 Yamadaoka, Suita City, Osaka 565-0871, Japan*

[b]*Department of Clinical Disorder Research, The Osaka-Hamamatsu Joint Research Center for Child Mental Development, Osaka University, 2-2 Yamadaoka, Suita City, Osaka 565-0871, Japan*

Abstract—Protein arginine N-methyltransferase (PRMT) 8 was first discovered from a database search for genes harboring four conserved methyltransferase motifs, which shares more than 80% homology to PRMT1 in amino acid [Lee J, Sayegh J, Daniel J, Clarke S, Bedford MT (2005) PRMT8, a new membrane-bound tissue-specific member of the protein arginine methyltransferase family. J Biol Chem 280:32890–32896]. Interestingly, its tissue distribution is strikingly restricted to mouse CNS. To characterize the function in the CNS neurons, we raised an antiserum against PRMT8 to perform immunohistochemistry (IHC) and Western blot analysis. By IHC, the immunoreactivity of endogenous PRMT8 was broadly distributed in the CNS neurons with markedly intense signals in the cerebellum, hippocampal formation, and cortex, but was not detected in the cerebellar granular layer. In some subset of the neurons, the immunoreactivity was observed in the dendrites and axon bundles. The subcellular localization of the immunoreactivity was dominantly nuclear, arguing against the original report that exogenously expressed PRMT8 localizes to the plasma membrane via the N-terminal myristoylation. A series of the exogenously expressed proteins with different in-frame translation initiation codons was tested for comparison with the endogenous protein in molecular size. The third initiator codon produced the protein that was equivalent in size to the endogenous and showed a similar localizing pattern in PC12 cells. In conclusion, PRMT8 is a neuron-specific nuclear enzyme and the N-terminus does not contain the glycine end for myristoylation target.

Key words: PRMT8, subcellular distribution, protein methylation.

Arginine dimethylation is a common modification of specific proteins by which two methyl groups are introduced from S-adenosyl-L-methionine (AdoMet) to either one of (asymmetric) or each of (symmetric) the terminal nitrogen atoms of the guanidine group of arginine (Paik and Kim, 1980; Aletta et al., 1998; Bedford and Richard, 2005). The reactions are catalyzed by protein arginine N-methyltransferases (PRMTs) of which nine family members have been identified in mammals (Bedford, 2007; Bedford and Clarke, 2009). They are categorized into type I and type II, according to whether they catalyze production of asymmetric (ADMA) or symmetric dimethylarginine (SDMA) on the target proteins, respectively. PRMT1, −3, −4, and −6 are classified into type I enzyme, while PRMT5 and −7 are classified into type II. Other members, PRMT2 and −9 are shown to have no detectable activity (Bedford, 2007; Krause et al., 2007; Bedford and Clarke, 2009). The functional involvement of PRMTs has been studied from various aspects of biological processes, transcriptional regulation (Chen et al., 1999; Covic et al., 2005; Yadav et al., 2008; Zhao et al., 2008), chromatin remodeling (Stallcup, 2001; Pal and Sif, 2007), DNA repair (Charier et al., 2004; Boisvert et al., 2005), signal transduction (Blanchet et al., 2005; Yamagata et al., 2008), RNA processing (Boisvert et al., 2002; Cheng et al., 2007), and translation (Swiercz et al., 2005). The regulatory system and the substrate selection of PRMTs have been rapidly elucidated in the last decade, but their biological functions have been poorly studied on brain tissue that has been known to abundantly contain methylated proteins (Paik and Kim, 1969; Kakimoto, 1971).

PRMT8 was first discovered from database search for novel open reading frames (ORFs) that harbor a highly conserved methyltransferase domain (Lee et al., 2005). An ORF, registered as hnRNP methyltransferase-like (Hrmt1l) 3 and 4 in the cDNA database, shows significant homology (more than 80%) with PRMT1 and was renamed as PRMT8. The striking feature of the gene is its expression pattern; the transcript of PRMT8 is limitedly expressed in the CNS, though the other family members are ubiquitously distributed among organs (Lee et al., 2005; Taneda et al., 2007). *In vitro* methylation assay demonstrated that the recombinant PRMT8 produced ADMA on H4 histone protein with a weaker activity than the endogenous modifier, PRMT1 (Lee et al., 2005; Sayegh et al., 2007). The deduced amino acid sequence predicted a longer N-terminal stretch than PRMT1, which contains an N-terminal glycine residue that functions as myristoylation site. As expected, the overexpressed protein was distributed along the membrane of HeLa cells, depending on the N-terminal glycine (Lee et al., 2005). According to the recent reports, the overexpressed PRMT8 in HEK293 cells or the recom-

*Corresponding author. Tel: +81-6-6879-3221; fax: +81-6-6879-3229.
E-mail address: mori@anat2.med.osaka-u.ac.jp (Y. Mori).

Abbreviations: ADMA, asymmetric dimethylarginine; BSA, bovine serum albumin; CPu, caudate putamen; EWS, Ewing sarcoma oncoprotein; HS, horse serum; IHC, immunohistochemistry; ISH, *in situ* hybridization; mAb, monoclonal Ab; Mo5, motor trigeminal nucleus; ORF, open reading frame; PAGE, polyacrylamide gel electrophoresis; PBS, phosphate-buffered saline; PNS, postnuclear supernatant; PRMT, protein arginine N-methyltransferase; RMC, reticular nucleus; RT, room temperature; SNR, substantia nigra; VPL, ventral posterior lateral nucleus of thalamus; 6N, abducens nucleus; 12N, hypoglossal nucleus.

0306-4522/09 $ - see front matter
doi:10.1016/j.neuroscience.2009.06.061

binant protein pulled down Ewing sarcoma oncoprotein (EWS) RNA-binding protein, which was mono- or dimethylated by PRMT8 (Pahlish et al., 2008). Since EWS was colocalized with PRMT8 on the plasma membrane, it is one of possible candidates for endogenous substrate. But these findings were gained from the artificial PRMT8 whose translation was initiated from the 5′-most in-frame AUG codon found on the native transcript. For this reason, there has been no information on endogenous PRMT8 until now.

To solve the problem, we raised a specific antiserum against PRMT8. The purified antibody recognized 42 kDa protein on SDS-PAGE that was observed exclusively in the brain lysate. Immunohistochemistry (IHC) analyses demonstrated that the immunoreactivity was distributed throughout mouse CNS, except for the cerebellar granule cell layer, and the positive cells expressed neuron-specific markers. To our surprise, the signal was dominant in the nuclei of the neurons and being concentrated in the progress of postnatal stage, arguing against the previous reports that the overexpressed PRMT8 was localized to the plasma membrane. To unravel the discrepancy, we explore the possibility that the proposed translation initiation site for the expression of PRMT8 was not the case in the physiological condition. Mentioned above, the expressed protein was translated from the hypothetical initiator codon that produced the common myristoylation site at its N-terminus. We made a series of expression constructs that were translated from the proposed initiator codon and the two downstream AUG codons in a Kozak's sequence-dependent manner and compared the molecular size of each of the expressed proteins with that of endogenous protein. The results demonstrated that the major form of endogenous PRMT8 was comparable to the expressed protein with the third initiator codon, which does not produce the N-myristoylation target that would be translated from the 5′-most initiator. In conclusion, PRMT8 is a neuron-specific protein that shows a dominantly nuclear distribution.

EXPERIMENTAL PROCEDURES

Generation of antiserum against PRMT8

Rabbits were immunized with a keyhole limpet hemocyanin (KLH)–conjugated peptide that corresponds to 55–71 amino acid sequence of PRMT8, NH_2-CPGRGKMSKLLNPEEMT-COOH (Lee et al., 2005), by Medical Biological Laboratories Company., Ltd. (Nagano, Japan). The antiserum was partially purified with Affi-gel 102 Gel (Bio-Rad, Hercules, CA, USA) that was conjugated with immunizing peptide.

Reagents and antibodies

We used the following antibodies: anti-PRMT1 polyclonal antibody (Upstate Biotech, Charlottesville, VA, USA), anti-tau monoclonal Ab (mAb; Upstate Biotech), anti-NeuN mAb (Sigma-Aldrich, St. Louis, MO, USA), anti-MAP2 mAb (Sigma-Aldrich), anti-APC mAb (EMD Chemicals Inc., Darmstadt, Germany), anti-GFAP mAb (Chemicon Interntional Inc., Temecula, CA, USA), anti-HA mAb (Sigma-Aldrich), anti-H3 histone polyclonal antibody (Cell Signaling Technology Inc., Danvers, MA, USA), anti-GAPDH mAb (Santa Cruz Biotech Inc., Santa Cruz, CA), Alexa 488–conjugated goat anti-rabbit IgG antibody, and Alexa 568–conjugated anti-mouse goat IgG antibody (Molecular Probes Inc., Eugene, OR, USA). The reagent used in this work was as follows: 2.5S mouse NGF (Upstate Biotechnology).

Cell culture

PC12 cells were grown in Dulbecco's Modified Eagle's Medium, supplemented with 10% horse serum (HS), 5% fetal calf serum, 100 U/ml penicillin, and 100 μg/ml streptomycin. Cells were cultured in a humidified 37 °C incubator with a 5% CO_2 atmosphere. The cells were incubated with 100 ng/ml NGF in DMEM supplemented with 1% HS for differentiation.

Western blot analysis and immunoprecipitation (IP)

The extracts from brain and other organs were prepared by washing the tissues three times with 0.02 M phosphate-buffered saline (PBS; pH 7.4) and then lysed with a Teflon homogenizer in an ice-cold TNE buffer (20 mM Tris–HCl (pH 7.5), 0.15 M NaCl, 1 mM EDTA containing 1 mM o-phenylmethylsulfonyl fluoride (PMSF)). The samples were clarified by centrifugation for 10 min at 17,400×*g* at 4 °C. The samples were normalized for protein content using the DC Protein Assay (Bio-Rad Laboratory). Aliquots of the protein extracts were mixed with Laemmli loading buffer for 30 min at 4 °C, separated by 10% SDS–polyacrylamide gel electrophoresis (PAGE), followed by transfer to a polyvinylidene difluoride (PVDF) membrane (Millipore, Billerica, MA, USA). The membranes were incubated with a blocking reagent (GE Healthcare Bio-Sciences Corporation, Piscataway, NJ, USA) for 1 h at room temperature (RT) and incubated with the primary antibodies for 12 h at 4 °C in 0.02 M PBS containing 0.05% Tween20 (PBS-T). The immunodetection was performed using the ECL Western Blotting Detection System (GE Healthcare Bio-Sciences Corporation) with horseradish peroxidase (HRP)–conjugated anti-rabbit IgG (Cell Signaling Technology), according to the manufacturer's instructions.

Immunoprecipitation assay was performed on the brain extract. The 50 μg of lysate was precleared with Protein G agarose (GE Healthcare Bio-Sciences Corporation) in TNE buffer for 2 h at 4 °C and centrifuged at 2000 rpm for 2 min. Thirty microliters of Protein G agarose was added to the supernatant with either control rabbit IgG or anti-PRMT8 antiserum and incubated overnight at 4 °C. The agarose was washed seven times with the TNE buffer and denatured in Laemmli loading buffer. The precipitated proteins were separated by SDS-PAGE and blotted with anti-PRMT1 polyclonal IgG (1:1000).

Plasmid construction

A series of plasmids that are translated from three different initiation codons in a Kozak's sequence-dependent manner was generated by a PCR-based method. We prepared three respective forward primers, 5′-aagcttccaccatgggcatgaaacactcctcccgctgcctgctc-3′ (1st), 5′-aagcttccaccatgaaacactcctcccgctgcctgctc-3′ (2nd), and 5′-aagcttccaccatggcggagaatgcagtcgaaagcac-3′ (3rd) (the numbering is referred to Fig. 5A; the possible initiator codons are underlined). The reverse primer was designed as follows; 5′-gaattcttagatatcacgcattttgtagtcattagatac-3′. Using the three primer sets, PCR reaction was performed on mouse brain cDNA as template. The products were subcloned into pGEM-T vector (Promega Corporation, Madison, WI, USA), and sequenced from T7 and SP6 promoters by ABI PRISM™ genetic analyzer (Applied Biosystems, Foster City, CA, USA). The subcloned fragment was cloned into pcDNA3.1 vector (Invitrogen, Carlsbad, CA, USA) with HindIII and EcoRI site (pC-MT8; 1st, 2nd, 3rd).

To purify recombinant PRMT8 proteins, PCR was performed using a primer set, 5′-ggatccggcatgaaacactcctcccgctg-3′ (forward) and 5′-gaattcacgcattttgtagtcattag-3′ (reverse) toward PC-MT8 1st plasmid. The amplified product was cloned into pGEX4T-1 (GE Healthcare Bio-Sciences Corporation) with BamHI and EcoRI

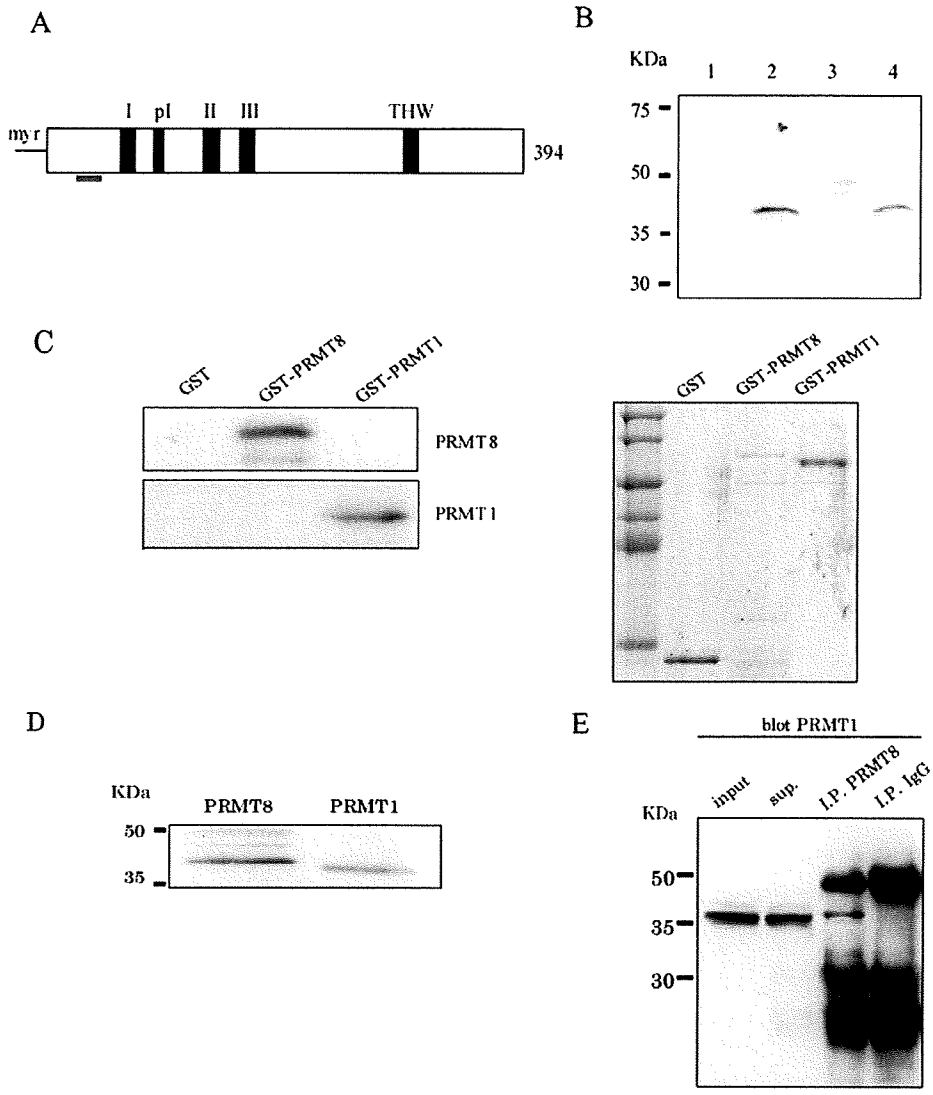

Fig. 1. Characterization of anti-PRMT8 antibody. (A) PRNT signature motifs in PRMT8. Motif I, post I, II, and III and THW loop are indicated. The selected immunogen are underlined by a red bar. (B) PRMT8 protein detected by Western blot analysis from mouse brain lysate. Lane 1: preimmune serum, lane 2: anti-PRMT8 antibody, lane 3: addition of excessive GST-PRMT8, lane 4: addition of GST alone. (C) Anti-PRMT8 antibody recognized GST-PRMT8, not GST-PRMT1 or GST alone (upper panel, left). Anti-PRMT1 antibody did not cross-react with GST-PRMT8 (lower panel, left). The right panel shows Commassie staining of the gel identical to that shown in the left panel. (D) Comparison of the anti-PRMT8 immunoreactive band with anti-PRMT1 counterpart. Mouse brain lysates were separated by SDS-PAGE in parallel lanes and transferred to membrane. The slower migrating band was detected with the antibody, rather than anti-PRMT1. (E) PRMT8 coprecipitated with PRMT1. Mouse brain lysate was loaded directly (input) or immunoprecipitated with anti-PRMT8 antibody. Rabbit IgG was used as respective negative control. The precipitated proteins were analyzed by immunoblotting with anti-PRMT1 antibody.

not show any immunoreactivity (Fig. 3A, column 5). These observations ensured that the immunostaining resulted from the specific recognition of endogenous PRMT8. However, the immunoreactivity was concentrated on the nuclei of the positive cells (Fig. 3A), arguing against the previous report that exogenously expressed PRMT8 is recruited to the plasma membrane by modification with myristoyl group on the N-terminus of PRMT8 (Lee et al., 2005). This discrepancy will be discussed below.

As well as the dominant nuclear signals in the neurons, some bundles of axonal fiber were immunostained with the purified antibody. The preeminent example is the cerebellar white matter where the tau-positive descending axons of Purkinje cells exhibited unambiguous immunoreactivity along their whole extension (Fig. 4A, 2nd row, arrows in inset of the merged view). Though not evident, the region ranging from the hilus to the stratum lucidum of the hippocampal CA3 region displayed the immunoreactivity of PRMT8 (Fig. 4, 1st row, CA3). The stratum lucidum corresponds to the synapse locations between mossy fiber terminals and dendrites of CA3 pyramidal neurons and therefore contains both axonal and dendritic components.

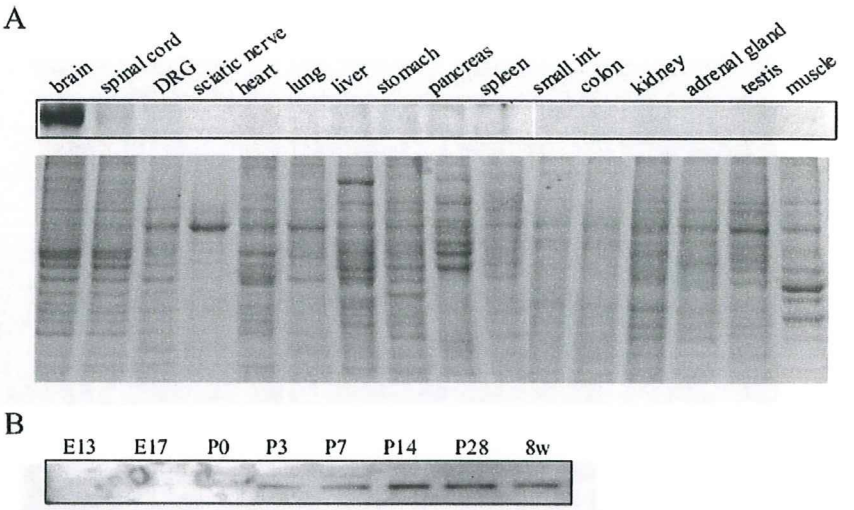

Fig. 2. (A) PRMT8 protein is expressed in brain and spinal cord. We performed Western blot using protein from a number of different mouse tissues. PRMT8 protein expression was only detected in the brain and spinal cord. The lower panel shows Commassie staining of the gel identical to that shown in the upper panel. (B) Ontogenetic expression of the PRMT8 protein in the mouse brain. The immunoreactivity was detected from a postnatal day 3 animal and peaked at postnatal day 28.

To elucidate the identity of the signals in the stratum lucidum, double staining with tau and MAP 2 was performed. The observed fibrillar immunoreactivities of PRMT8 were tau-positive (Fig. 4, 1st row, merged view), while they exhibited a mutually exclusive distribution with MAP 2-positive region (Fig. 4, 3rd row). Other fiber systems, such as anterior commisure and corpus callosum, exhibited the signals at the background level (data not shown).

To reconfirm the subcellular localization of PRMT8, cytoplasmic and nuclear fractions were prepared from 14-day-old mouse brain tissue. PRMT8 was immunodetected in the nuclear fraction, with a comparable level of signal in the cytoplasmic fraction (Fig. 4B, lanes N and C). This result is consistent with IHC data on the nuclear localization of PRMT8, but does not correspond to the much lower level of cytoplasmic IHC signals. Considering stringent separation of the nuclear and cytoplasmic fraction by respective marker proteins (Fig. 4B, middle and lower panels), it is possible that PRMT8 might leak out from the nuclei by the fractionation procedures.

Distribution of PRMT8-positive neurons in mouse brain

The PRMT8-positive cells were broadly distributed throughout the mouse brain, in the olfactory bulb, cortex, hippocampal formation, basal ganglia, thalamic nuclei, nuclei of midbrain and brainstem, cerebellum, and spinal cord. The regional differences in signal intensities were paralleled to those from *in situ* hybridization (ISH) data (Taneda et al., 2007), despite the subtle discrepancies in relative intensities of some brain subregions. From the ISH data, the cell populations of interconnected nuclei that belong to the special and general somatosensory afferents, limbic system, and corticostriatal circuitry were labeled with relatively higher intensity. On the other hand, some of the somatomotor nuclei, habenular nucleus, mammillary body, substantia nigra (SNR), accessory olfactory bulb, medial septum, and red nucleus exhibit no detectable or, if any, faint, signals from PRMT8 transcript. However, by means of fluorescence IHC, contrasts of the immunostaining were not so outstanding that the brain regions and subregions could be graded into multiple groups on the basis of their signal intensities. Table 1 recapitulates the IHC results by classifying the brain areas into two groups with apparently high and low signal intensities of their component cells (Table 1). In Fig. 5, typical IHC views of the high and the low intensity groups are shown; basal ganglia including caudate putamen (Fig. 5A, CPu), reticular nucleus (Fig. 5C, RMC), SNR (Fig. 5D), hypoglossal nucleus (Fig. 5F, 12N) are classified into the low intensity group, while ventral posterior lateral nuclei of thalamus (Fig. 5B, VPL) and motor trigeminal nucleus (Fig. 5E, Mo5) into the high intensity group. The IHC signals were substantially detected even in the brain regions that do not contain the ISH signals, like brainstem somatomotor nuclei including oculomotor, abducens, trochlear, hypoglossal (Fig. 5F), and ambiguous nuclei. Notably, abducens nucleus (6N) exhibited the strong IHC signal, despite no detectable ISH signal.

Cerebellum is the region with the highest immunoreactivity. Particularly, Purkinje cells showed the strongest signal among the anatomical regions in the CNS (Fig. 4A, 2nd row, PC) and the significant level of immunoreactivity was observed in the dendrites of the Purkinje cells (Fig. 4A, 2nd row, arrowheads in inset on Mo). Other cells in the cerebellum, like basket cells, satellite cells, and Golgi cells, also displayed nuclear immunoreactivities to lesser extents. It should be noted that the cererbellar granule cell layer possessed no detectable level of immunoreactivity, except for some of the scattered cells that are presumed to be interneurons (Fig. 4A, 2nd row, Gr).

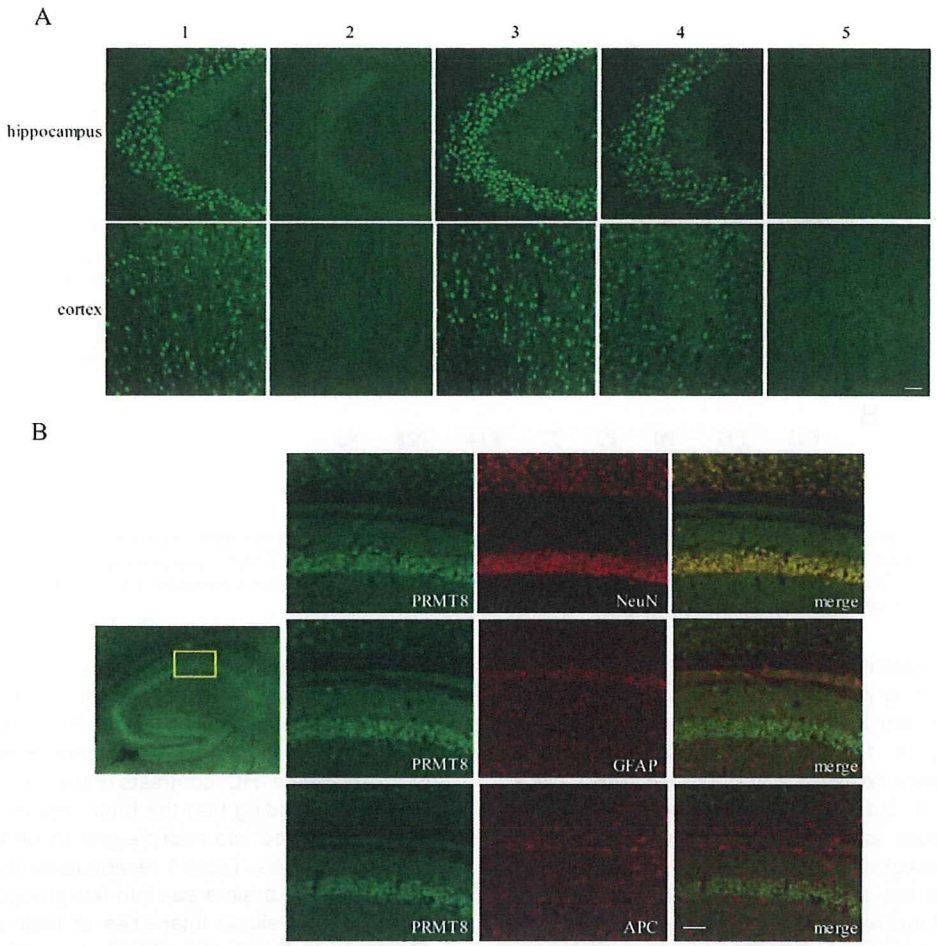

Fig. 3. Immunocytochemistry of PRMT8 in mouse brain. (A) 1: Anti-PRMT8 antibody, 2: anti-PRMT8 adsorbed with recombinant PRMT8, 3: anti-PRMT8 antibody with recombinant GST alone, 4: anti-PRMT8 antibody with recombinant PRMT1, 5: preimmune serum. The signal was depleted with the addition of PRMT8 antigen. Preincubation with recombinant PRMT1 had no effect on the immunoreactivity. (B) PRMT8 was expressed in neuronal cells. Fluorescence IHC was performed using anti-PRMT8 (green), anti-NeuN (red), anti-GFAP (red) and anti-APC (red) antibodies on mouse brain. Scale bar=50 μm.

The lineage of PRMT8-expressing cells

To examine what lineages of cells express PRMT8, the brain sections were costained with PRMT8 antibody and lineage-specific markers, NeuN, GFAP, and APC. In the hippocampal sections, all the PRMT8-positive cells stringently overlapped with NeuN-positive neuronal cells in the pyramidal and granule cell layers (Fig. 3B, 1st row). The dendritic marker, MAP2, was localized to the same cells with PRMT8-positive nuclei (Fig. 4A, 3rd row). On the other hands, GFAP- and APC-positive cells showed no overlap with the PRMT8-positive cells that are located along the stratum oriens (Fig. 3B, 2nd and 3rd rows), demonstrating that the expression of PRMT8 is neuron-specific.

Ontogenic analysis of PRMT8 expression in the mouse brain

Using the antibody against PRMT8, the ontogenic expression in the mouse brain was analyzed by Western blot (Fig. 2B). PRMT8 was detectable from the first few days after birth and gradually increased with developing stages, which peaked at the second postnatal week. The higher level of PRMT8 expression in the adulthood was also confirmed by IHC (Fig. 7), suggesting physiological functions of PRMT8 in the mature brain.

The physiological N-terminus of PRMT8

The original report on PRMT8 demonstrated that, when overexpressed in HeLa cells, it was localized on the plasma membrane via N-terminal myristoyl chain that is added to the glycine residue next to the initiator methionine (Lee et al., 2005). However, they designed the expressed PRMT8 that was translated in frame from the 5′-most initiator codon (referred to 1st, Fig. 6A) to produce the myristoylated glycine residue and the following N-terminal myristoylation consensus sequence (Lee et al., 2005). In fact, two candidate initiators exist in frame downstream of the first initiation codon, neither of which would translate glycine residue as myristoylation target (Fig. 6A). Thus,

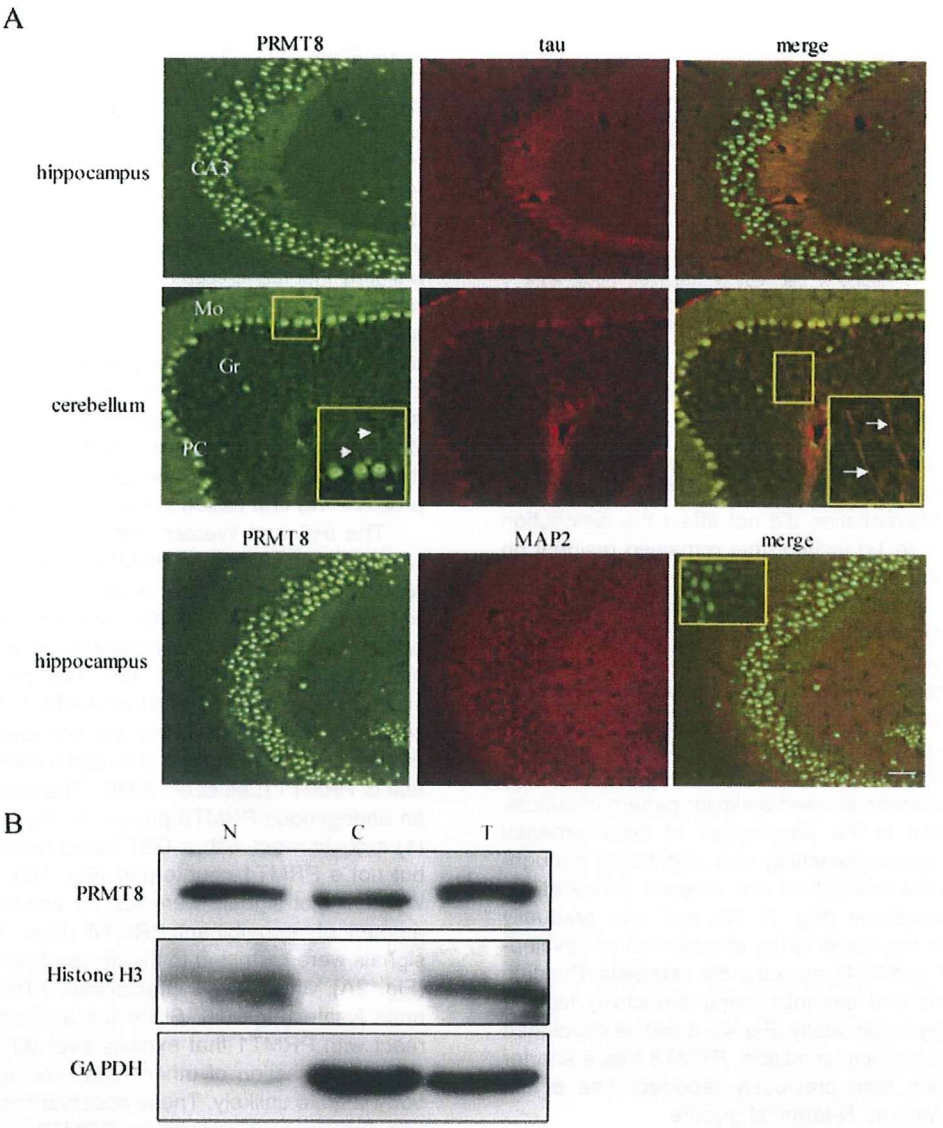

Fig. 4. PRMT8 was localized in nuclei and axon. (A) Fluorescence IHC was performed using anti-PRMT8 (green), anti-tau (red) and anti-MAP2 (red) antibodies on the hippocampal and cerebellar sections. In the cerebellum, PRMT8 immunoreacivity was significantly detected along the dendritic arbors (arrowheads in inset) and the descending axons of Purkinje cell (arrows in inset). The anti-PRMT8 signals well overlapped with tau-positive regions. Scale bar=50 μm. (B) Subcellular fractionation assay. N, nuclear fraction; C, cytoplasmic fraction; and T, total lysate were prepared from P14 mouse brain tissues and blotted with anti-PRMT8 antibody.

unless the 1st in-frame AUG was selected as initiator codon, the second residue was not read out as glycine to which the myristoyl chain is covalently linked (Lee et al., 2005). Given that our IHC data exhibited nuclear-dominant distribution of the immunoreactivity, this raised the possibility that a bona fide PRMT8 is translated from the second or third AUG to produce a myristoylation-free protein.

To explore the effect of the translation initiation codons on subcellular localization of the proteins, we made a series of constructs expressing hypothetical PRMT8s that were artificially translated from the 1st, 2nd, and 3rd initiation codons in a Kozak sequence-dependent manner (Fig. 6A). These plasmids were transfected into PC12 pheochromocytoma cells that exhibited no positive signal with the antibody. We first blotted aliquots of the lysates from each of the transfectants and compared the apparent sizes of the exogenous products with the endogenous one. Expectedly, the product from the 3rd initiation codon showed a faster mobility shift than the others (Fig. 6B). The fluorography showed that the apparent size of the endogenous PRMT8 was comparable to the product from the 3rd initiation codon (Fig. 6B, compare 3rd Met and brain lysate).

Next, the subcellular localization of each of the products with different initiator codons was examined by IHC. In the proliferative condition, the protein translated from 1st initiator was mainly distributed on the plasma membrane of the PC12 cells (Fig. 6C, 1st Met), while those from the 2nd

Table 1. Distribution of the cells expressing PRMT8 in the mouse brain

Density grade	Representative region
High	Mitral cells, piriform septum, hippocampus, thalamic N, amygdala, mesencephalic N of trigeminal n (5N), interpeduncular N, pontine N, 6N, superior olivary N, facial N (7N), ventral and dorsal cochlear N (8N), vestibular N, cuneate N.
Low	CPu, SNR, red N, the colliculus, tegmental N, raphe N, ceruleus N, trapezoid body, area postrema, dorsal N of vagus n (10N), lateral reticular N, 12N, inferior olivary N, solitarii N, cerebellar N, etc.
No fluorescence	Cerebellar granule cells

N, nucleus and nuclei; n, nerve.

and 3rd initiators were wholly distributed in the cells somewhat in a nuclear-dominant pattern (Fig. 6C, the top row). NGF-induced differentiation did not affect the distribution of the proteins with 1st initiator that remained resident on the plasma membrane. This observation suggested that the expressed protein was actually lipidated at the N-terminus and anchored to the plasma membrane (Fig. 6C, 1st Met). Interestingly, the proteins with the 2nd and 3rd initiators were concentrated on the nuclear compartment in the course of the differentiation (Fig. 6C, 2nd and 3rd Met). More than 90% of cells exhibited nuclear-dominant pattern five days after the NGF treatment. The ontogenic pattern of subcellular localization showed a similar pattern of subcellular translocation in the progression of developmental stage. PRMT8 immunoreactivity was distributed throughout the cells in the cerebellum and cerebral cortex at the onset of its expression (Fig. 7, P0) and was gradually concentrated on the nuclei in the progression of development (Fig. 7, P7 and P14), except in the cerebellar Purkinje cells with axonic and dendritic immunoreactivity leaving positive at 14 days postnatally (Fig. 4). It can be concluded that, in the physiological condition, PRMT8 has a shorter N-terminal stretch than previously reported (Lee et al., 2005) possibly with no N-terminal glycine.

DISCUSSION

To search for a clue to elucidate functions of protein arginine methylation in the CNS, we focused on the executing enzymes, PRMTs, that reside in the brain region. In general, the PRMT family is ubiquitously-distributed enzymes that exhibit no organ-specific expression with varying expression levels among different organs. However, the only exception is PRMT8 that is specifically expressed in the CNS (Lee et al., 2005). Therefore, functional analysis of PRMT8 would lead to an advanced understanding of the physiological significance of protein arginine methylation in the CNS. Previous reports on PRMT8 demonstrated that the enzyme possesses a type I methyltransferase activity that produces ADMA residues on GAR-like motifs and H4 histone protein *in vitro* (Lee et al., 2005; Sayegh et al., 2007). The striking feature of PRMT8 is its membranous localization, as deduced from its amino acid sequence with a highly conserved myristoylated site at the N-terminus (Lee et al., 2005). As PRMT8 interacting partner, a recent proteomics approach identified some proteins with RGG motifs that are preferentially targeted by type I arginine dimethylation and are shared by a wide range of RNA-binding proteins. One of the interactants, EWS was effectively mono- or dimethylated by PRMT8 *in vitro* methylation assay and was colocalized with the transfected PRMT8 on the membrane of HEK293 cells (Kim et al., 2008; Pahlish et al., 2008). However, since there has been no available antibody that recognizes PRMT8, characterization of endogenous PRMT8 remained to be done. Hence, the previous studies have accumulated information on the exogenously expressed protein that is translated from the 5′-most initiation codon that would follow the methylatransferase motifs in frame (Lee et al., 2005; Sayegh et al., 2007; Pahlish et al., 2008) and failed to confirm whether the used initiator was the case or not in the physiological condition. To solve the problem, we first raised the antiserum against PRMT8.

The IHC and Western blot data in this study agreed with previous studies on PRMT8, except that the immunoreactivity was observed predominantly in the cell nuclei (discussed below). The antibody exclusively detected a protein with 42 kDa of apparent molecular mass from mouse brain lysate (Fig. 1B). The protein exhibited a slightly slower mobility shift than PRMT1 (Fig. 1D), which is consistent with the fact that the deduced amino acid sequence of PRMT8 harbors a longer N-terminal stretch than that of PRMT1 (Lee et al., 2005). The antibody recognized an endogenous PRMT8 protein for the following reasons: (1) it could react with a GST-fused recombinant PRMT8, but not a PRMT1 counterpart (Fig. 1C), (2) the IHC and Western blot signals were lost by addition of the excess amount of recombinant PRMT8 (Figs. 1B, 3A), (3) the signals were restricted to the mouse brain and spinal cord (Fig. 2A), and (4) it coprecipitated PRMT1 from mouse brain lysate (Fig. 1E). Since the antibody did not cross-react with PRMT1 that exhibits over 90% homology with PRMT8, detection of other PRMT members by the antibody is quite unlikely. These observations were consistent with the previous reports on PRMT8 (Lee et al., 2005), supporting the antigen specificity of the antibody. The immunolabeled cells were well overlapped with neuronal cell markers, NeuN and MAP2, demonstrating that PRMT8 is one of the neuron-specific enzymes (Fig. 3B).

IHC signals were distributed throughout the brain, with marked immunoreactivity observed in the hippocampus, cerebral cortex, and cerebellar Purkinje cell layer (Table 1). However, no positive cells were observed in the cerebellar granule cell layer where the ISH signal was also undetectable (Fig. 4A, Taneda et al., 2007). The immunopositive cells were detected even in the regions with relatively weak transcript levels, including SNR (Fig. 5D), habenular nuclei, mammillary body, medial septal nuclei, red nucleus, and some somatomotor nuclei in the brainstem (Table 1). The 6N exhibited robust immunostaining, despite having no ISH signals (Table 1, Taneda et al., 2007). This disagreement between the IHC and ISH data might be responsible for the higher sensitivity of fluorescent signals than that of radiopositive signal by ISH; alter-

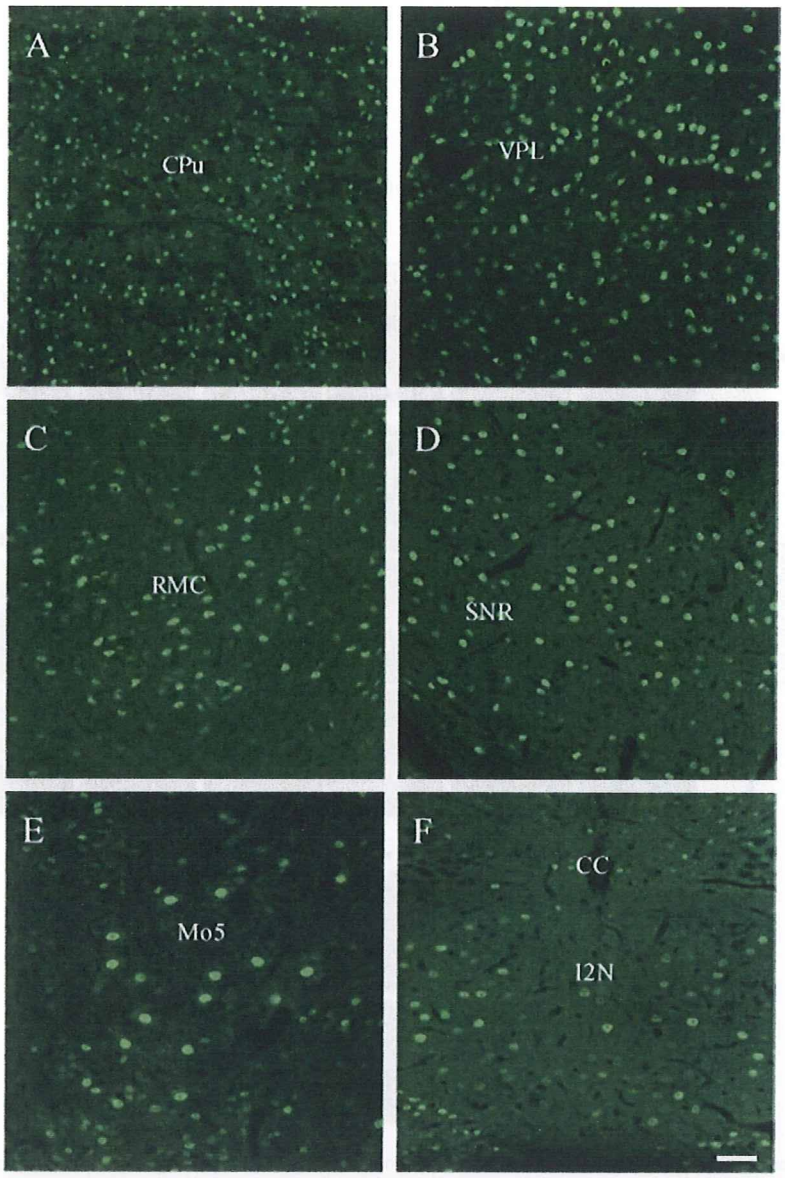

Fig. 5. Immunohistochemical views of mouse brain regions. (A) CPu, (B) VPL, (C) RMC, (D) SNR, (E) Mo5, (F) 12N. As classified in Table 1, VPL and Mo5 belong to the high expression group of PRMT8. For interpretation of the references to color in this figure legend, the reader is referred to the Web version of this article.

natively, posttranscriptional regulation of the transcript is regionally varied, which might in turn mediate a higher translation level of the transcript or a longer decay rate of the protein in the above regions.

Involvement of the translation initiation site of PRMT8 in its subcellular localization

The most unanticipated result was the predominantly nuclear distribution of the IHC signals in the neurons (Figs. 3–7). Tissue fractionation assay demonstrated that PRMT8 was distributed equally in the nuclear and cytoplasmic fractions (Fig. 4B). The cytoplasmic population was presumably due to the leakage from the nucleus by the experimental procedures, because the fractions were completely separated in terms of the distribution of marker proteins. These results supported that notion that PRMT8 is a nuclear protein, inconsistent with previous reports that overexpressed PRMT8 was localized to the plasma membrane as a myristoylated protein (Lee et al., 2005). Though the cytoplasmic immunoreactivity was observed in the axons and dendrites of the strongly labeled neurons (Fig. 4A), the staining was diffusely and evenly distributed over the cells with no membrane-delineated signal characteristic of myristoylated proteins (Figs. 4 and 7). If PRMT8 transcript is translated from the 5′-most initiator codon (Fig. 6, 1st), the next glycine residue would be myristoy-

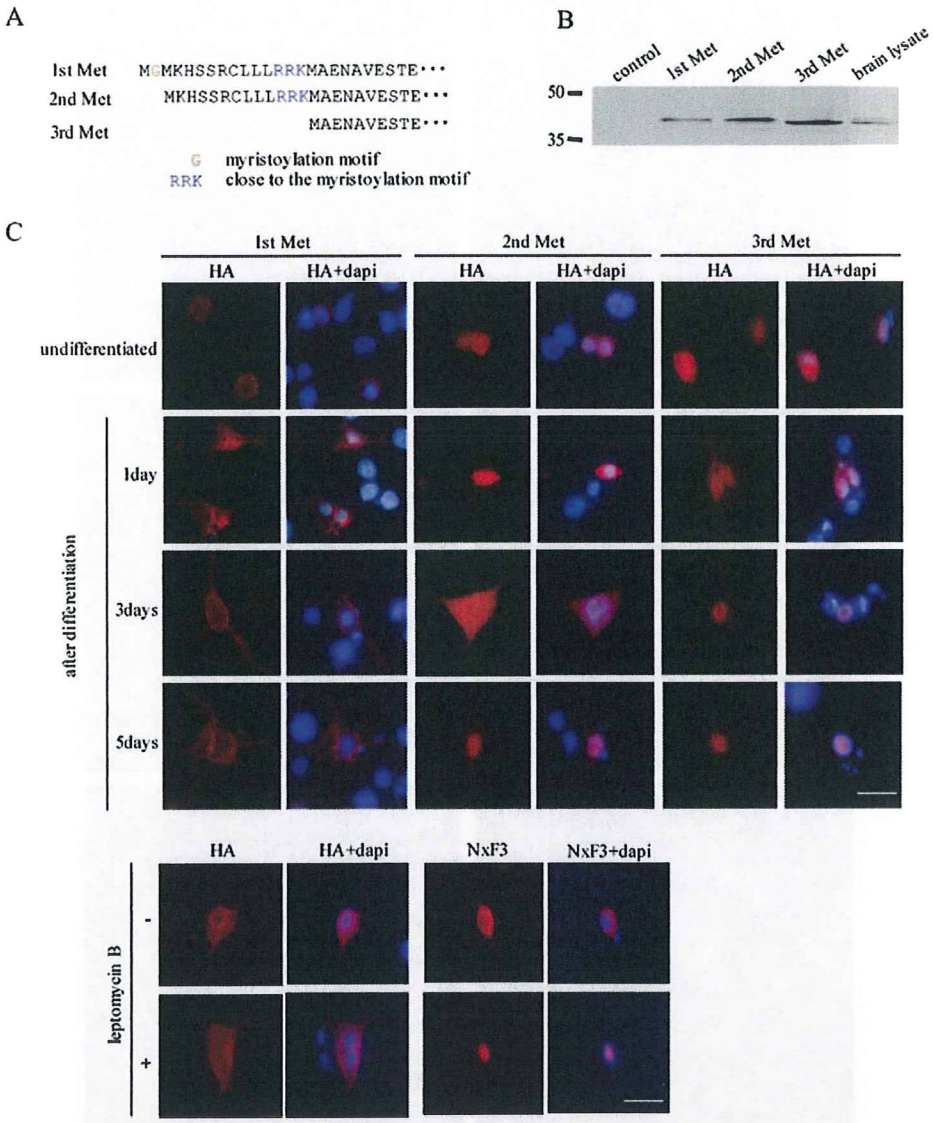

Fig. 6. Subcellular localization of PRMT8. (A) Sequence of the putative N-terminal ends of PRMT8. The protein with 1st initiator codon harbors N-terminal glycine residue (1st Met) for myristoylation. 2nd and 3rd initiators do not generate the structure at their N-termini (2nd and 3rd Met). (B) Comparison of apparent molecular size of endogenous PRMT8 with those of the expressed proteins with three different initiator codons represented in (A). PC12 cells were transfected with either of the plasmids expressing the protein with different initiators. Anti-PRMT8 blot showed that the endogenous PRMT8 (brain lysate) was comparable to the protein with 3rd Met in size. (C) Change in the subcellular distribution of three expressed PRMT8 species in PC12 cells after NGF-induced differentiation. 1st Met PRMT8 was absolutely localized at the plasma membrane even after the differentiation. In contrast, 2nd and 3rd Met PRMT8s were concentrated on the nuclei in the progression of differentiation. Scale bar=20 μm.

lated by the aid of the following sequence that mediates the modification. Hence, we speculated that the hitherto assumed initiation site of PRMT8 (1st Met) was not physiological. To test the possibility that other in-frame initiator codons are used for translation, we constructed PRMT8 expressing vectors whose transcripts were translated from three of the putative initiator codons driven by Kozak sequence (Fig. 6A). Downstream of the 1st in-frame AUG, two candidate initiators exist at the third and sixteenth methionine from the 1st initiator (Fig. 6A). When the proteins were overexpressed in PC12 cells, the 1st initiator codon recruited the protein to the plasma membrane as reported previously (Fig. 6C). However, such membranous localization was not observed for the proteins translated from both of the 2nd and 3rd initiators that would not follow the N-terminal common myristoylation site. Instead, these proteins were localized to the nuclei and cytoplasm of the PC12 cells that were cultured in the growth condition (Fig. 6C). After NGF-induced differentiation, a significant proportion of PRMT8 was concentrated on the nuclei (Fig. 6C), consistent with the alteration of subcellular distribution in the course of brain maturation (Fig. 7). These observations implied that PRMT8 was translated from other initiator codon(s) than the 1st in-frame AUG. Western blot data